Autofocusing and image segmentation in microscopy for automatic detection of tuberculosis in sputum smears

---

Prepared by:

Megan J. Russell

Biomedical Engineering

Department of Human Biology

University of Cape Town

South Africa

Supervisor:

Dr. Tania S. Douglas

This thesis is submitted in partial fulfilment of the requirements for the degree of Master of Science in Medicine (MSc (Med)), Biomedical Engineering.

15 March 2006

SYNOPSIS

The World Health Organisation (WHO) has declared that tuberculosis (TB) is a global emergency. With the common combination of TB and AIDS in sub-Saharan Africa, the number of people dying from TB has increased enormously (WHO, 1996).

The smart microscope that is under development in the MRC/UCT Medical Imaging Research Unit would considerably aid the fast detection and tracking of TB. The microscope will automatically detect the presence of TB bacilli in Ziehl-Neelsen (ZN) stained sputum smears. The microscope consists of a digital camera, motorised stages, and will have an on-board processor containing the algorithms for autofocusing the microscope and for automatically identifying TB bacteria on the slides.

This thesis deals with autofocusing the microscope and segmenting TB bacilli from focused sputum smear images

Autofocusing of the Smart Microscope

Passive autofocusing was the method chosen for use with the smart microscope. This involved the use of a focus measure to indicate whether the image was in-focus or not. Three focus measures were considered:

- Energy of the Image Laplacian
- Variance of the Log-Histogram
- First Order Gaussian Derivative

These focus measures were tested on sequences of slides, ranging from out-of-focus to in-focus to out-of-focus again. The Energy of the Image Laplacian was chosen as it performed well with a short processing time.

Once a suitable focus measure had been chosen, the next step was to design a search algorithm that would find the position of optimal focus. Two different search methods were combined, namely sequential step searches followed by the fitting of a quadratic curve to find the maximum focus measure and thus the point of optimal focus.

The results for the autofocus algorithm were good, with a maximum discrepancy in focus position of 4μm between the algorithm and the author. However the algorithm does take longer to focus than other systems reported in the literature.

Segmentation of Images from the Smart Microscope

Image segmentation can be performed on grey-scale or colour images and has been classified into a number of different approaches by different authors in literature. In this thesis, grey-scale and colour segmentation of images from the smart microscope were investigated.

- **Grey-Scale Segmentation:** Crisp and fuzzy thresholding techniques were investigated with no real difference found between the results of the two. The TB bacteria were not segmented from the rest of the image.

- **Colour Segmentation:** Three different colour segmentation techniques were investigated, namely: colour edge extraction, Canny edge detection and colour compensation thresholding.
  1. The colour edge extraction method either over-detected or vastly under-detected the images, with no happy medium in between. This method is not suitable for use with images from the smart microscope.
  2. Canny edge detection worked well on images taken by the smart microscope. This is the method favoured in the literature covering the field of image segmentation for the detection of TB bacilli. However the method cannot differentiate between TB bacteria and other types of bacteria or other objects in the image.
  3. Colour compensation thresholding is a novel method. This method worked the best out of the three colour image segmentation methods. The matrix that was created specifically for the colour of the TB bacteria in the images from the smart microscope ensured that only the TB bacteria were detected and not other types of bacteria or other objects. This is the recommended image segmentation method for use with the smart microscope.

Conclusions

An autofocusing algorithm has been developed and tested for the smart microscope. The algorithm works satisfactorily for all of the slide series on which it was tested, but it does run more slowly than autofocusing algorithms reported in the literature. The developed algorithm uses the Energy of the Image Laplacian focus measure and does not use windowing. An autofocusing algorithm for ZN stained sputum slides has never been investigated before.

Both Canny edge detection and colour compensation thresholding are suitable for use on sputum smear images that contain TB bacilli. However the colour compensation thresholding method gives slightly better and more specific results than the Canny operator as it segments bacilli only. The colour compensation thresholding method is a new segmentation method based on the colour compensation technique proposed by Castleman (1993).

The following conference paper resulted from this work:

M. J. Russell, A. Bester and T. S. Douglas, "Autofocusing a smart microscope for the detection of tuberculosis in sputum smears", *Proceedings of Sixteenth Annual Symposium of the Pattern Recognition Association of South Africa*, 23-25 November 2005, Langebaan, South Africa, pp 183-189

ACKNOWLEDGEMENTS

Thanks to Dr. Tania Douglas for enthusiastically supervising this thesis.

Thanks to Andre Bester for designing and building the smart microscope.

Thanks to Dr. Genevieve Learmouth for sharing her knowledge and providing invaluable advice about TB.

Thanks to Mrs Bosman at the Greenpoint Laboratories for providing the sputum slides.

DECLARATION

I, Megan J. Russell, hereby declare that the work, on which this thesis is based, is my own original work (except where acknowledgements indicate otherwise) and that neither the whole, nor any part of it, has been or will be submitted for any other degree at this or any other university.

Signed by candidate

Signed

15-03-06

Date

TABLE OF CONTENTS

LIST OF FIGURES

LIST OF TABLES

1 INTRODUCTION

1.1 BACKGROUND TO STUDY

The World Health Organisation (WHO) has declared that tuberculosis (TB) is a global emergency. With the common combination of TB and AIDS in sub-Saharan Africa, the number of people dying from TB has increased enormously. Currently the health services are overwhelmed with the number of people suffering from TB. This leads to problems such as a high mortality rate during treatment, a low TB cure rate, high rates of re-infection and high rates of drug resistance. The diagnosis of TB is also compromised due to lab technicians being overworked; thus there is an over-diagnosis of sputum smear-negative TB and under-diagnosis of sputum smear-positive TB (WHO, 1996).

The smart microscope that is under development in the MRC/UCT Medical Imaging Research Unit would considerably aid the fast detection and tracking of TB. The microscope will automatically detect the presence of TB bacilli in sputum smears. The microscope will consist of a digital camera, motorised stages, and a processor that will contain the algorithms for autofocusing the microscope and for automatically identifying TB bacteria on the slides. Representative images of the slides will be stored for human review.

The smart microscope would contribute to superior TB control in the following ways:

- It would form the basis for a low-cost microscope substitute for use in any TB screening laboratory with access to electricity.
- It will allow a greater number of slides to be screened, thus increasing the screening efficiency and reducing the demands on laboratory staff.
- Reduced human involvement in the screening process will mean that less technically experienced staff could perform TB screening.
- Reduced human involvement could reduce the risk of laboratory staff contracting TB.
- It will be able to scan a greater number of fields with higher diagnostic accuracy.

This thesis deals with automatic focusing of the microscope and the segmentation of TB bacilli from focused images of Ziehl-Neelsen stained sputum smears.

1.2 OBJECTIVES

Autofocusing for microscopy is a well established field; however there is not one general solution for all autofocusing problems. Most autofocus algorithms are image and purpose specific. Thus the main problem addressed in this proposal is to create a fast, reliable autofocusing algorithm

that is suitable for the subsequent detection of TB bacilli in Ziehl-Neelsen stained sputum smears. This objective can be broken down into:

1. Finding the best focus measure
2. Finding the most appropriate search algorithm to locate the position of optimal focus
3. Comparing the efficacy of the autofocusing algorithm with manual focusing.

Segmentation involves the separation of objects in the image from each other and the background. The segmentation objective is to find a segmentation algorithm that can successfully distinguish between the TB bacilli and other objects in the image.

1.3 THESIS OUTLINE

- **Chapter 2** – This chapter gives an outline of tuberculosis and its impact on Southern Africa. An introduction to automated microscopy is also given and a number of different uses of automated microscopy are also shown.
- **Chapter 3** – This chapter contains the literature review for autofocusing. Sputum smear microscopy for TB detection and passive and active autofocusing methods are discussed as well as other topics that must be considered in the design of an autofocusing algorithm.
- **Chapter 4** – The autofocusing algorithms tested for use with the microscope are outlined.
- **Chapter 5** – The results of applying the algorithms described in Chapter 4 are presented and discussed.
- **Chapter 6** – This chapter contains the literature review for image segmentation. Grey-scale and colour image segmentation methods are discussed as well as colour spaces and other related topics.
- **Chapter 7** – The methods used for bacillus segmentation namely grey-scale and colour image segmentation algorithms are outlined.
- **Chapter 8** – The results of the image segmentation algorithms are presented and discussed.
- **Chapter 9** – General conclusions on autofocusing and segmentation and recommendation for further work are given.

1.4 LIMITATIONS

The following limitations were encountered in this project:

- The MATLAB programming environment could not be used to control the camera and microscope directly. Thus the autofocusing and segmentation algorithms were tested on either individual images of slides or images from sets of slides.
- Only a limited number of sputum smear positive slides could be procured in time for this project from the Greenpoint Laboratory.
- The quality of the slides was variable. Some sputum smears were stained well and were thinly smeared on the slide, thus making image analysis easy. Other smears were badly stained and inconsistently smeared, thus increasing the difficulty in obtaining good images.

1.5 INTRODUCTION TO EQUIPMENT

The following equipment was used to perform the autofocusing and segmentation algorithms:

- A laptop computer running the Microsoft Windows XP operating system with a 1.59 GHz Intel Pentium processor and 512MB RAM. The programming environment used was MATLAB 6.5 Release 13. Control software for the microscope was developed by Andre Bester, formerly a member of and currently a consultant to the MRC/UCT Medical Imaging Research Unit.
- A 'smart' microscope (see Figure 1) which consisted of a light microscope with a 40x 0.65 N.A objective lens and a slide stage that could move in the x-, y- and z-axes. Zaber T-LA Linear Actuators were used to control the stage and were connected to the computer through a serial port. A Lumenera digital camera (model LU200) was attached to the eyepiece of the microscope. The camera communicates with the computer via a USB port. The control software for the microscope (see Figure 2) was used to move the stage to the required x-, y- and z-coordinates and to capture images using the camera. The 'snapshot' function in the camera interface allows images from the camera to be saved in a number of different file formats (such as JPEG and BMP). These images could then be imported into MATLAB. The camera had a 2.0 megapixel sensor and produced images with a resolution of 1600 x 1200 pixels using 8 bits per pixel per colour. Each pixel was 4.2μm square.
- Slides with varying amounts of image density were used. These slides were obtained from the Tuberculosis Laboratory at the National Health Laboratory Service in Greenpoint, Cape Town.

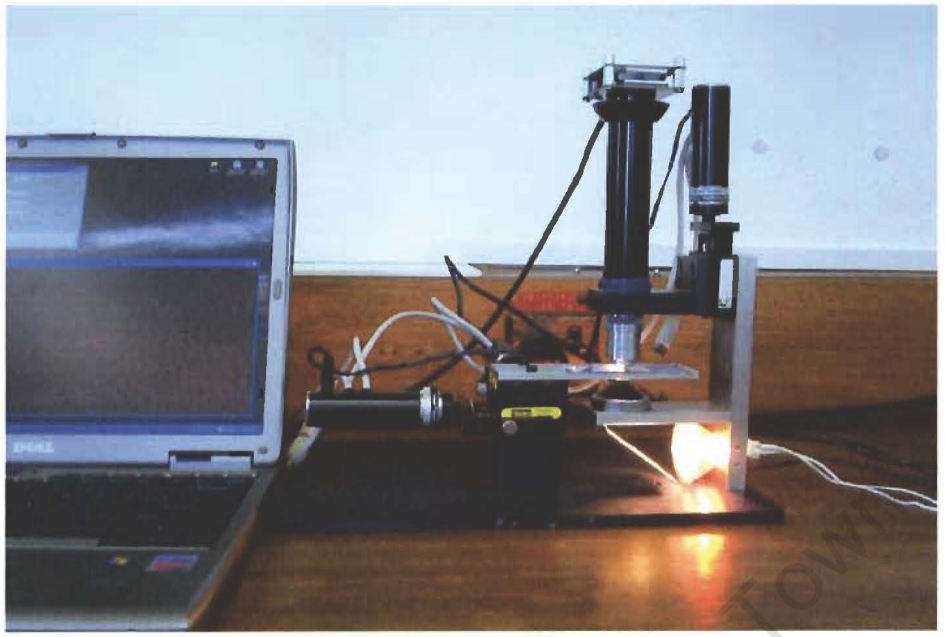

Figure 1 The current smart microscope

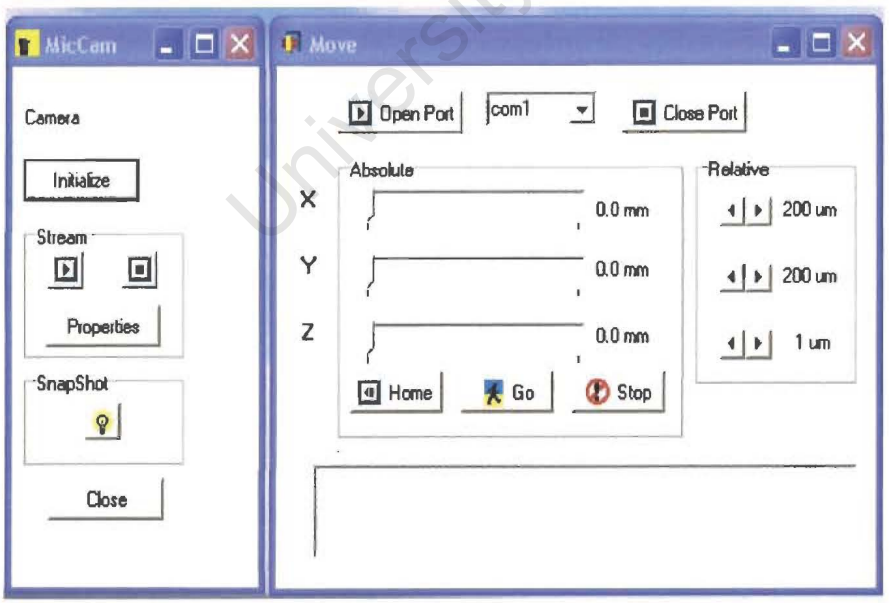

Figure 2 The user interface for the camera control software. 'MicCam' was the software to control the camera. 'Move' was the software to control the stage actuators.

Images from sources other than the smart microscope were used to test some of the algorithms developed, especially in the image segmentation section. These were taken from a previous thesis by Edlauer (2004).The images were taken using a conventional professional research light microscope with the Lumenera LU200 camera mounted on it. A 40x 0.65 N.A. objective lens was used.

2 BACKGROUND TO TUBERCULOSIS AND AUTOMATED MICROSCOPY

Tuberculosis (TB) is an infectious disease caused by the micro organism *Myobacterium tuberculosis*. The micro organism usually enters the body through inhalation into the lungs. It can then spread to various other sites in the body. There are two types of tuberculosis (IUATLD, 2000):

- **Pulmonary Tuberculosis**: This accounts for more than 80% of diagnosed cases. It is the infectious form of TB. Transmission of TB occurs by the airborne spread of infectious droplets coughed out of the lungs by a person infected with TB.
- **Extra-pulmonary Tuberculosis**: This is when tuberculosis affects organs outside of the lungs. TB can affect any organ in the body but it most often affects the spine, genitals, lymph nodes, neural system or abdomen.

Without treatment, 50% of people infected with TB die within 5 years, 25% will have cured themselves (they possess a strong immune system) and 25% will have chronic, infectious TB (WHO, 1996).

2.1 SPUTUM

Sputum is matter that is coughed up from the lower airways of the respiratory track. It consists of mucous or phlegm that may be mixed with saliva from the mouth. Sputum can contain pus, blood, bacterial products, fibrin (a protein involved in the clotting of blood) and other foreign bodies (Merriam-Webster, 2005).

2.2 TUBERCULOSIS DIAGNOSIS

Every person suspected of having TB must have a sputum examination test to determine whether or not they have infectious TB. This must be done before treatment can commence. The examination consists of taking a sample of sputum from the patient, spreading it on a microscope slide and then staining it with a Ziehl-Neelsen (ZN) stain or an auramine stain. The ZN stain causes the bacilli to turn reddish-pink and the background to turn blue while the auramine stain causes the bacilli to fluoresce against a dark background (see Figure 3). A light microscope is used to detect bacilli in ZN stained smears and a fluorescent microscope detects bacilli in auramine-stained smears. If micro organisms are detected using either method, the patient is said to have smear positive TB. This method efficiently identifies the cases of TB which are most infectious and thus allows priority of treatment to be given (IUATLD, 2000). The difference between the stains can be seen in Figure 3. Fluorescent microscopes have a more complex design

than light microscopes which increases their cost and their maintenance requirements. The method of choice in low-income countries where TB is rife is therefore light microscopy of ZN stained specimens (Ulunkanligil et al., 2000).

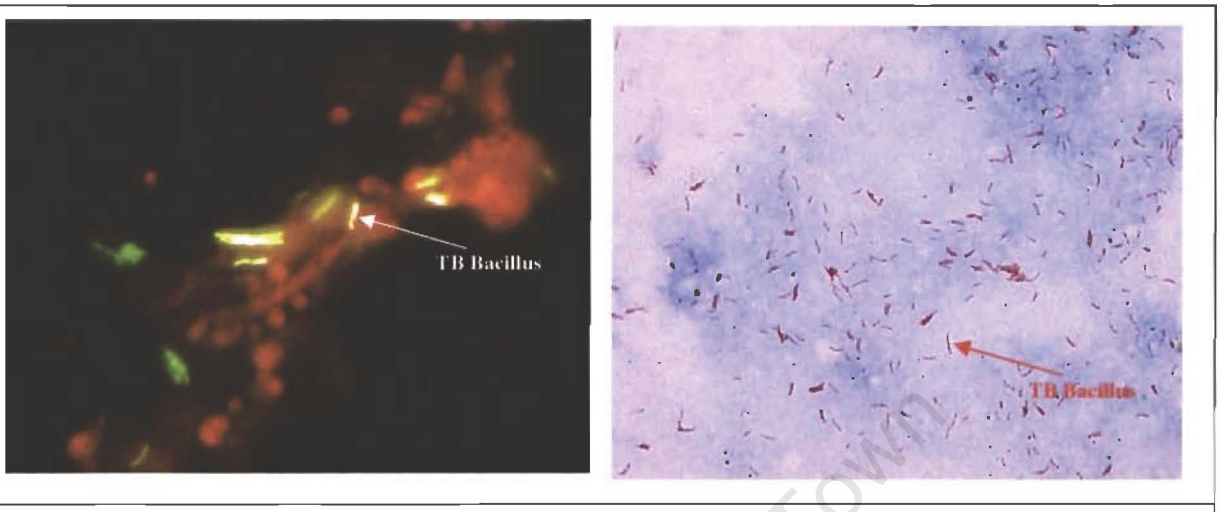

Figure 3 An example of an auramine stain on the LHS (Forero et al., 2001) and a ZN stain on the RHS (Veropoulos, 2001)

2.3 HIV/AIDS AND TUBERCULOSIS

A healthy, HIV-negative person has a lifetime risk of 5-10% of contracting TB, however a HIV-positive person has a lifetime risk of 50%. Thus many people infected with HIV contract TB (WHO, 1996). In an individual with HIV, the presence of TB and other infections causes the HIV to progress to AIDS much more quickly than it would have had the patient been otherwise healthy. Because of the HIV-positive patient's weakened immune system, cases of extra-pulmonary TB are a lot more common. The presence of the HIV virus and a dampened immune system also causes the progression from TB infection to infectious TB disease to occur faster. This means that in a community with a high number of HIV-positive individuals, the number of infectious TB cases is increasing, thus increasing the risk of exposure to uninfected members of the community.

In 2004 South Africa was rated as the country with the 9th highest incidence of TB in the world. 60% of South African adults diagnosed with TB are HIV-positive (see Figure 4).

SOUTH AFRICA

LATEST ESTIMATES[a]	
Population	44 759 187
Global rank (by est. number of cases)	9
Incidence (all cases/100 000 pop)	558
Incidence (new ss+/100 000 pop)	227
Prevalence (ss+/100 000 pop)	192
TB mortality per 100 000 pop	79
% of adult (15-49y) TB cases HIV+	60
% of new cases multi-drug resistant	1.5

Figure 4 Latest estimates for TB in South Africa by WHO (2004).

In developing countries, TB is the single most common cause of death for people aged between fifteen and forty-nine years (IUATLD, 2000).

2.4 The Health Infrastructure and TB Treatment

The impact of the HIV epidemic in sub-Saharan Africa exposes shortcomings in the current TB treatment campaign of the region, as people with HIV are more prone to contracting TB. This rise in TB suspects is putting a strain on diagnostic services (WHO, 1996). The consequences of overloading diagnostic services are the following (WHO, 1996):

- Over-diagnosis of sputum smear-negative Pulmonary TB
- Under-diagnosis of sputum smear-positive Pulmonary TB
- Inadequate supervision of patients taking their anti-TB drugs
- Low cure rates
- High mortality rates during treatment
- High rates of TB recurrence
- Increased emergence of drug resistance.

It is necessary to find and treat people with TB accurately and quickly. Identification of TB is routinely done by analysing sputum smears with a microscope. However, manual screening for the bacilli is labour intensive and there is a high false negative rate (Forero et al., 2004).

A microscope technician analysing TB slides is expected to take at least 5 minutes per slide and look at 100 fields on the slide. Industry standards state that a single technician should not process more than 25 ZN stained slides a day. Table 1 indicates the manner in which TB sputum smear slides are graded.

Table 1 IUATLD-recommended grading of sputum smear microscopy results. (AFB stands for Acid Fast Bacilli (i.e. those causing TB), the number of +'s grade the severity of the TB infection)

AFB counts	Recording/reporting
No AFB in at least 100 fields	0/negative
1 to 9 AFB in 100 fields	Actual AFB counts
10 to 99 AFB in 100 fields	+
1 to 10 AFB per fields in at least 50 fields	++
> 10 AFB per field in at least 20 fields	+++

2.5 AUTOMATED MICROSCOPY

In recent years a number of automated microscopy systems have been developed. Many tasks in microscopy rely on a technician to identify and count abnormal cells or objects present in a sample. A number of these types of applications are open to automation. The following are some examples of automated microscopy designed to lessen the technicians screening time and load:

- One of the most widely known and utilised systems is the Papnet® system, designed to automate the microscopic screening for cervical cancer in pap smears. Using a neural network, the Papnet® system identifies up to 128 abnormal looking cells in a Pap smear and stores the images for re-screening by a trained technician. With conventional screening, much of a technician's time is spent assessing normal smears. With Papnet®, a suitably trained technician can assess 2 to 3 times as many smears as in the conventional manner (Prismatic, 1999).
- Microscopic examination of urine sediment is a crucial element in the diagnosis and tracking of renal diseases but it can be time-consuming and inaccurate. Thus the iQ200 automated urine microscopy analyser has been developed. It analyses the unspun urine and provides results comparable to manual methods but with a more rapid turnaround time (Lamchiagdhase et al., 2005).
- Circulating tumour cells can be observed at very low concentrations in the blood of cancer patients. The number of these cells is known to correlate with the outcome of patients with breast cancer that has metastasised. Automated digital microscopy is used to recognise and count the number of immunochemically labelled tumour cells (Hsieh et al., 2006).

2.6 REQUIREMENTS OF AUTOMATED MICROSCOPY

Requirements of an automated microscopy system vary depending on the application. However a number of features are required for most systems:

1. **Autofocusing**: This ensures that the specimen is in correct focus.
2. **Image acquisition**: This can generally be done by using a digital camera or any other CCD device. Filters may or may not be used.
3. **Image processing**: This step is the most varied. Image processing can consist of filtering, segmentation, clustering, morphological operators and many other operations. The image processing step generally prepares the image for neural network analysis.
4. **Neural networks**: These are trained to recognise the object that the system was designed to detect. They can be single- or multi-layer.
5. **Storage:** This involves the storing of suspect images for subsequent review by a technician.

2.7 AUTOMATED BACILLUS DETECTION

Steps 3 and 4 in Section 2.6 have been used in TB detection. Both Forero et al. (2004) and Veropoulos et al. (1998) developed bacillus-detection techniques that automatically detect TB bacilli in sputum samples stained with fluoroscope auramine. Forero et al. (2004) obtained sensitivity of 73.3% to 100%, and specificity of 88.7% to 99.7% on a per view field basis in detecting TB bacilli. Veropoulos (1998) found sensitivity of 93.53% and specificity of 98.79% on a per bacillus basis. Sensitivity is the ratio of true positive decisions against the number of positive cases and specificity is the ratio of true negative decisions against the total number of negative cases.

These bacillus detection techniques potentially have many advantages in TB screening. These advantages include decreased workload for technicians and improved sensitivity and accuracy in diagnosis due to the increased number of images the computer can scan. However, the fluorescence microscope used to analyse the auramine stained smears in this technique is prohibitively expensive, and is therefore not suited for low-income countries. ZN stained sputum analysis is done on a light microscope, which is far more accessible to low-income countries.

To date, only a preliminary study, on a small number of images, has been conducted on the automatic detection of TB bacilli in ZN stained sputum smears (Veropoulos, 2001). An overall accuracy, sensitivity and specificity of 79.9%, 83.7% and 76.4% respectively, were found on a per bacillus basis.

3 AUTOFOCUSING LITERATURE REVIEW

3.1 INTRODUCTION

Automatic detection of bacilli requires a number of different steps. The first is to ensure that the microscope correctly autofocuses the slides. This means that the slides are always kept in optimum focus. The other steps in automatic detection concentrate on the image processing of the final image and the detection of bacilli, however these are beyond the scope of this literature review. Many different autofocus algorithms have been developed. Unfortunately very few papers (Della Mea et al., 2005, McKeogh et al., 1995, Nicolls, 1995, Boddeke et al., 1997, Geusebroek et al., 2000, Forero et al., 2004) deal solely with the autofocusing of a microscope, as most of the main research into autofocusing has been directed towards cameras. Nevertheless a number of the algorithms developed for cameras are still applicable and will be considered here.

In general there are two ways to approach autofocusing. The first involves using a predefined focus measure which is applied to images captured at different positions of the lens with respect to the slide. The resulting focus measure values are then searched to find the optimal focus position. This is known as passive autofocusing. The second approach uses knowledge of the image formation process to find the degree of defocus in the images. This is known as active autofocusing (Nicolls, 1995).

3.2 IMAGE FORMATION

Image formation through a convex lens (similar to that in a simple camera) is shown in Figure 5.The focused lens position v depends on the distance u to the object to be focused and the focal length f of the lens. They are related by the Gaussian lens law:

$$\frac{1}{f} = \frac{1}{u} + \frac{1}{v}$$

If the object is moved from the focused position u then a defocused image will appear on the image plane. The problem in autofocusing is to find a position where the image is best focused from a series of images obtained at different values of u.

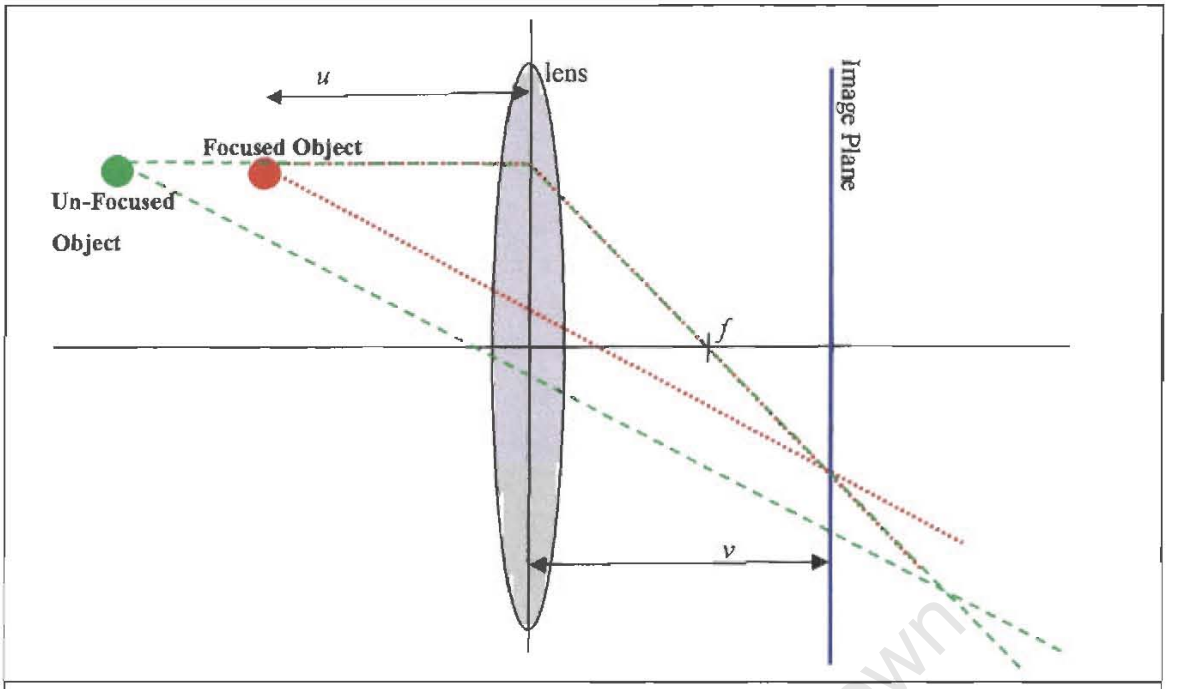

Figure 5 Image formation through a convex lens. Adapted from Zhang et al. (2000)

3.3 PASSIVE AUTOFOCUSING

Passive autofocusing is also known as 'pixel-based autofocus'. It is flexible and easy to implement although it can be computationally expensive (Della Mea et al., 2005).

3.3.1 The Focus Measure

The focus measure is an indication of how in-focus an image is. Focus measures are generally Gaussian in shape, with the maximum point of the curve corresponding to the position of focus (see Figure 6). It can be obtained from the image in the following manner. First the image is normalised for brightness. It is then convolved with the focus measure filter (FMF) and the energy in the filtered image is computed (see Figure 7). This energy is the focus measure. Blurring an image is equivalent to passing it through a low pass filter (high frequency attenuation), thus most FMFs correspond to filters that emphasise high frequencies (Subbarao and Tyan, 1998). Different authors have proposed a number of different focus measures.

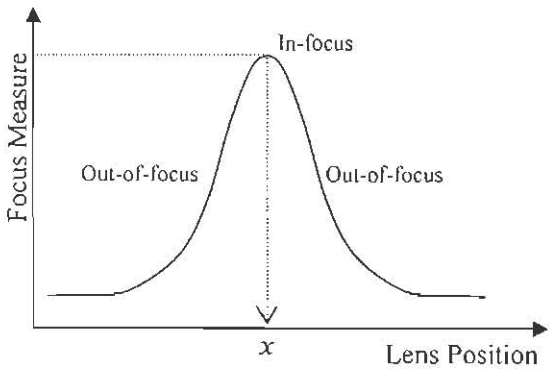

Figure 6 An example of an ideal focus measure. Note that the maximum focus measure occurs at the point when the image in focus.

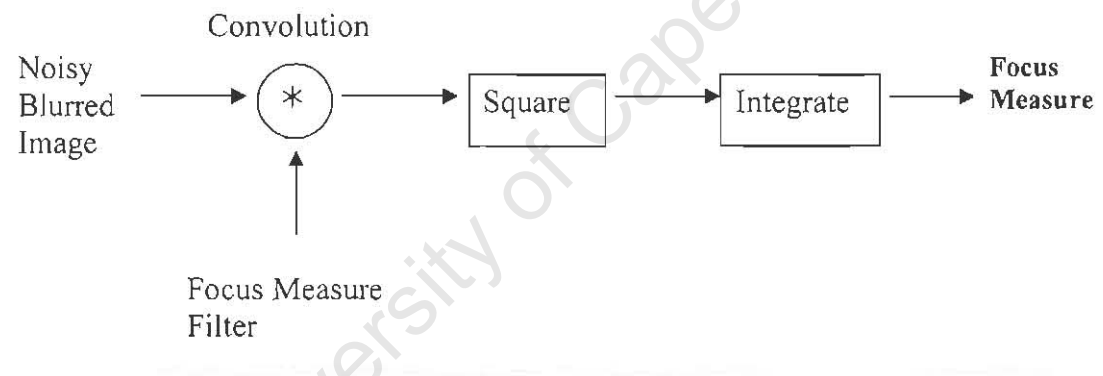

Figure 7 Model of a focus measure (Subbarao and Tyan, 1998).

According to Santos et al. (1997) focus measures can be grouped into five different classes depending on the information they use from the image. These are gradient, peaks/valleys, variance, histogram and correlation. Kautsky et al. (2002) laid out some basic requirements that all focus measures should follow. They state that it must be content independent (must not be based on any particularly bright structures in the image), it should be monotonic with respect to blur (the more blurred the image, the less the focus measure should be) and the measure should be robust to noise. Geusebroek et al. (2000) gives the following criteria for good focusing: accuracy, reproducibility, general applicability and insensitivity to other parameters.

Although autofocusing is a long standing topic in literature, there is no generally applicable solution. Methods are often designed for one kind of imaging mode (Geusebroek et al., 2000). Whilst developing their automatic TB detection algorithms, Forero et al. (2004) investigated four standard and one novel focus measure before designing their own. The techniques they used were: grey level variance, Energy of the Image Laplacian, a wavelet based measure and autocorrelation. They found that none of the measures provided meaningful results when applied to their data, as the contribution of the TB bacteria to the total image was so small. They found that the Variance of the Log-Histogram provided the best focus measure.

In an attempt to find a focus measure independent of the object to be imaged, Zhang et al. (2000) developed a focus measure method using statistical moments. However this moment-based measure is very sensitive to boundary effects and thus can only be used effectively on images that have no background (Kautsky et al., 2002).

Santos et al. (1997) recommended the use of the Vollath-5 (correlation based) measure as they showed it to have a high score in terms of accuracy, range, false-peaks and computation time. However, when this algorithm was implemented by Kehtarnavaz and Oh (2003) they found that the function did not produce a well defined peak and was noisy.

Della Mea et al. (2005) tested the squared magnitude-gradient, squared Laplacian, normalised image standard deviation and the Vollath F4 function (using variance and autocorrelation) on a large number of histologic and cytologic images. They found that the Vollath F4 was not effective on low content images, while the gradient and Laplacian functions were too sensitive to noise. However they also found that the Laplacian measure presented the best specificity in individuating the focus plane, a result noted by Subbarao et al. (1993) and Santos et al. (1997).

The only generally applicable solution for microscopy is given by Geusebroek et al. (2000), who proposed the use of a First-Order Gaussian Derivative to measure the focus score. They tested their autofocus algorithm on the following applications: neuronal morphology, cardiac myocyte differentiation, immunohistochemical label detection, screening of *C. elegans* worms (for transgenic worms expressing vulval muscles), acquisition of smooth muscle cells and immunocytochemical label detection. To evaluate the performance of the autofocusing algorithm unfocused, arbitrarily selected fields were visited and manually focused by two independent experienced observers. The focus positions were recorded for both observers and were then compared to the focus position found by the algorithm. The results showed a 98% to 100% success rate for bright light microscopy applications, a greater than 99% success rate for

fluorescent microscopy applications and a 100% success rate for phase-contrast microscopy applications.

3.3.2 Finding the Position of Optimal Focus

In real-time autofocusing applications, the bottle-neck is not caused by the computational time but rather by the time taken for the mechanical motion of the lens to move from one position to another (Subbarao and Tyan, 1998). Once the focus measure has been calculated for different positions of the lens with respect to the slide, the next step is to move the lens to the position of the optimal focus measure, thus ensuring that the system is in the correct focused position. A large number of different techniques can be used.

The most obvious method is global searching. In this technique the peak position is found by scanning though all lens positions in a forward manner. Thus there is no chance of falsely obtaining a local maximum. However this method is very slow and is only effective if the focus range is narrow as it is extremely computationally expensive (Kehtarnavaz and Oh, 2003).

The most computationally effective search algorithm is the Binary or Fibonacci search, which uses a 'divide-and-conquer' approach. However, as this method passes the optimal focus position every time, the mechanical motion is extensive which causes this method to be very time consuming (Svahn, 1996).

The 'difference of signs' approach computes the gradient of the function to be maximised and then moves in the negative direction. This involves computing the focus measure for one lens position, moving to another position and calculating the focus measure. The difference of the two focus measures is then obtained and if it is negative, the lens has moved in the wrong direction. Although this method is very simple to implement it can only be used for unimodal functions (Svahn, 1996).

Focus measure functions tend to take the shape of a Gaussian bell. Thus a function can be fitted to the collected data points and the maximum found. This maximum should correspond to the maximum of the focus measure (Svahn, 1996).

Subbarao and Tyan (1998) proposed an algorithm that combines a difference-of-signs, a coarse Binary or Fibonacci search and interpolation to minimise the lens motion. Initially a difference-of-signs is taken to indicate in which direction the lens should be moving. A coarse search is then performed in this direction to narrow the search interval. The focus measure is then taken at three

different points in this interval and a Gaussian curve is fitted to these points. The maximum of the Gaussian curve is taken to be the maximum focus measure.

3.4 Active Autofocusing

This method involves analysing the captured images and then relating them back to the system's parameters. Knowledge of the precise way in which the imaging system affects the image is required to relate information from the blurred image to a system parameter. The amount of defocus of an object in an image is often used to obtain the distance to the object. This depth-from-defocus approach can be used for autofocusing. By knowing the distance to the object the focal length can be corrected to bring the object into focus. A requirement of this method is a means of translating the amount of blur into the required variable (normally the distance to the object). There are two approaches to this translation: the use of look-up-tables or the use of models (Nicolls, 1995).

The advantage of active focusing is that the entire search process associated with passive focusing is avoided. The system can be focused by using information acquired from two or three lens positions (Subbarao and Tyan, 1998). However the system must be calibrated before the distance to the object and thus the focal length can be found (Nicolls, 1995). According to Subbarao and Tyan (1998) depth-from-defocus autofocusing methods are less accurate than search-based methods.

3.5 Backlash

Backlash is the difference in the physical position between approaching a motor position from above or from below. It is present in all microscope stages. To avoid backlash the motorised stage must approach the optimal focus position from the same side, preferably from below. If the stage is approaching from above, it must travel past the desired position by at least the size of the backlash before travelling up again. The backlash can be measured by comparing two focus functions. One is obtained from the successive images while moving the stage up and the other obtained from images while moving the stage down. The shift in the maximum values reached in the focus functions is the mechanical backlash (Boddeke et al., 1997). The actuators used for the smart microscope have an automatic 'anti-backlash' command, thus backlash is not an issue for the smart microscope.

3.6 Slide Quality

Passive autofocusing algorithms will fail to correctly focus a slide if there is a shortage of content in the field to be imaged. When the maximum focus measure found is not significantly larger than the measures at the end of the focus interval, the focus position must be rejected. The microscope

should then attempt to focus a neighbouring field (Geusebroek et al., 2000). If a predetermined number of fields do not contain enough content, the slide should be rejected and flagged for human inspection.

Besides shortage of content in the slide, a number of other factors can cause the autofocusing algorithm to fail. Examples of these factors are:

- Fingerprints on the glass cover
- Dust and dirt on the glass cover
- Bubbles and dust embedded between the cover and the slide.

These factors may cause the microscope to focus on them instead of the bacteria, thus causing the automatic detection algorithm to fail (Della Mea et al., 2005).

3.7 Depth of Field

The depth of field of an optical system is defined as the axial distance from the focal plane over which details can still be observed with satisfactory sharpness (Geusebroek et al., 2000), i.e. how far away from the optimal point of focus will objects in the image still look in focus. Depth of field can be found from the following equation (Geusebroek et al., 2000):

$$z_d = \frac{\lambda}{2n\left(1 - \sqrt{1 - (NA/n)^2}\right)}$$

where n is the refractive index of the medium, λ is the wavelength of the used light and NA is the numerical aperture of the objective lens.

The smart microscope uses an objective lens with a magnification of 40x and numerical aperture (NA) of 0.65. The NA is governed by the refractive index (n) of the medium between the front of the objective lens and the cover on the slide and the angle (θ) at which the light rays enter the objective lens.

$$NA = n \sin(\theta)$$

The medium between the objective lens and the slide cover is air, which has a refractive index of one. The wavelengths in the visible light spectrum range from 780nm (red) to 390nm (violet). Thus for red light the depth of field for the smart microscope is 1.6μm and for violet light 0.8μm.

3.8 CONCLUSION

Passive autofocusing algorithms are more appropriate than active autofocusing algorithms for the smart microscope as no calibration of the system is required. As the autofocusing algorithm needs to work quickly and accurately a focus measure and search algorithm should be chosen with care. As demonstrated above, what works well for one application may not be suitable for another application.

4 AUTOFOCUSING METHOD

4.1 AUTOFOCUSING ALGORITHM

A passive autofocus algorithm can be divided into two main components:

1. The focus measure
2. The search algorithm

Before the focus measure can be found the image of the slide must be acquired. This was done using the digital camera. The camera was controlled by a laptop computer and images were downloaded from the camera to the laptop. The images were then imported into the MATLAB programming environment. Each image was then converted from a colour RGB image to a greyscale image. Its brightness was then normalised by dividing the image by the mean of the image brightness. Once this was complete the focus measure of the image could be found. A more detailed description of the equipment used is given in Chapter 1.

4.1.1 Slide Series

As MATLAB 6.5 r13 cannot communicate with the USB port and therefore with the camera, a number of series of slides images were taken and then imported into MATLAB. Each of the series consisted of images taken out-of-focus, in-focus and out-of-focus again. See Table 2 for an example of selected slides from the test slide range. The test slide series alone contained over 80 separate images of a graduated test slide. The test slide series and a further 19 slide series of various specimens were used to test the autofocusing algorithm.

Table 2 An example of a slide series with images of a graduated test slide.

Blurry Image	Slightly In-focus Image	In-focus image	Slightly In-focus Image	Blurry Image
Image no: 63	Image no: 66	Image no: 72	Image no: 78	Image no: 81
		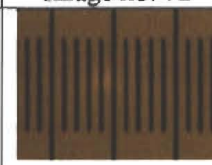	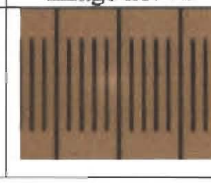	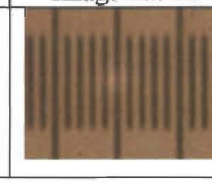

The smallest distance the actuator could move along the z-axis was 1μm. When the slides were very out-of-focus, images were captured 25μm apart. However, as the slides became more in-focus, images were captured every 1μm. The search algorithm (discussed later) took these varying distances between the images into account.

4.1.2 The Focus Measure

The focus measure can be found in many different ways. However according to Subbarao and Tyan (1998) the number of candidate focus measures that should be considered for good performance is limited. From the focus measures published for microscopy applications, those that might be suitable for ZN stained sputum slides, based on their generality or their previous use in bacillus detection in auramine-stained sputum slides, were selected. Thus the focus measures that were considered were:

1. **Energy of the Image Laplacian** (Subbarao and Tyan, 1998). This can be found by applying the following equation to the image:

$$M_L = \sum_{i,j} \left(g(i-1,j) + g(i+1,j) + g(i,j-1) + g(i,j+1) - 4g(i,j) \right)^2$$

where g(i,j) is the image's grey level function at pixel (i,j).

Subbarao and Tyan (1998) recommend the Energy of the Image Laplacian as a sound, unimodal and monotonic focus measure suitable for practical applications.

2. **Variance of the log-histogram** (Forero et al., 2004). The equation to find the Variance of the log-histogram is as follows:

$$M_{log} = \sum_{l} (l - E_{log}\{l\})^2 \log(p_l)$$

where p_l is the probability of intensity level l in the image and where

$$E_{log}\{l\} = \sum_{l} l \log(p_l)$$

is the expected value of the log-histogram.

As these equations were designed for use in fluorescence microscopy, the bacteria show up bright against a dark background. The reverse occurs in light microscopy, the bacteria are dark against a light background. Thus in order to apply the Variance of the log-histogram equations to a light microscopy image, the inverse of the image must be used instead of the original image.

Forero et al. (2004) used this focus measure in autofocusing their system for the automatic detection of tuberculosis using fluoroscope auramine.

3. **First Order Gaussian Derivative** (Geusebroek et al., 2000). This involves the convolution of each pixel in the image with the derivative of a Gaussian smoothing function at that point. The equation is:

$$F(\sigma) = \frac{1}{NM} \sum_{x,y} [f(x,y) * G_x(x,y,\sigma)]^2 + [f(x,y) * G_y(x,y,\sigma)]^2$$

where f(x,y) is the image's grey value at pixel (x,y) and $G_x(x,y,\sigma)$ and $G_y(x,y,\sigma)$ are the first order Gaussian derivatives in the x and y directions respectively, at a scale of σ (the standard deviation).

Geusebroek et al. (2000) presented this focus measure as a generally applicable focus measure for light microscopy. They achieved very good results whenever the image content was sufficient.

σ must be chosen such that noise in the image is maximally suppressed while the response to details of interest in the image is preserved. For bar-like structures such as TB bacilli an approximate value for σ can be found as follows (Geusebroek et al., 2000):

$$\sigma \approx (d/2)\sqrt{3}$$

where d is the thickness of the bar (which is ±4μm for TB bacilli).

The procedure for calculating the focus measure for all the images was timed, as calculation time is an important factor in choosing the best focus measure.

4.1.3 The Search Algorithm

Subbarao and Tyan (1998) recommended a combination of search algorithms to decrease the amount of lens movement. The following algorithm, based on their work, was used:

1. First the difference-of-signs method was used to move the lens in the correct direction. This was performed by finding the focus measure of the current position. The camera was then moved 25 μm along the z-axis and the focus measure found. This was repeated twice more in the same direction. The average of these focus measures was then found and compared to the first focus measure. If the average focus measure was larger, then the camera moved in the correct direction to focus the slide. If the average focus was smaller, then the camera had moved in the wrong direction and the opposite direction was

used to focus the microscope. The average of the focus measures was used to reduce the effects of noise.

2. A sequential search was then initiated by moving the lens in 25μm steps in the direction found by the difference-of-signs until the focus measure decreased by a preset amount for the first time (position D1). The search interval was then narrowed to 50μm before this point of decrease i.e. new interval = [D1 – 50; D1]. This ensured that the focus position lay within the interval.
3. A smaller sequential search was then performed in steps of 10μm from the start of this smaller interval (D1-50) until the focus measure decreased for the first time (D2). The search interval was then narrowed to 20μm from the point of decrease i.e. new interval = [D2 – 20; D2].
4. A quadratic curve was then fitted to three points inside this interval and the turning point found. This was the position of the maximum focus measure.

4.2 WINDOWING

Windowing involves performing the focusing algorithm on only a selected portion of the entire image. Seven different combinations of windowing were investigated to see whether they could reduce the time taken to focus the images. They are illustrated in Table 3.

Table 3 Illustration of the windowing operations

Windowing Operation	Example	Windowing Operation	Example
None – i.e. Original image x=1:1200 y=1:1600	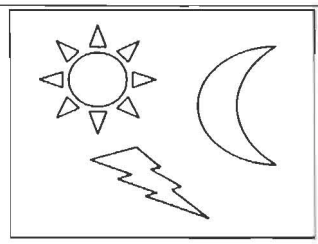	4 – **Rectangular Windowing** x=2:1199 y=602:989	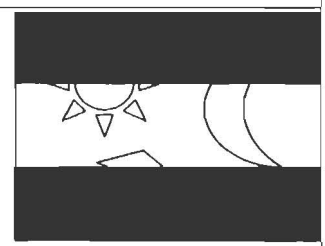
1 – **Square Windowing** x=302:898 y=302:1498	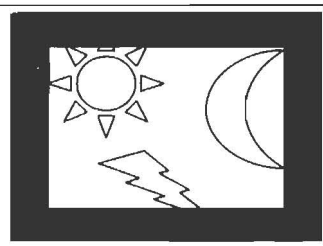	5 – **Every 6th line** x=2:6:1199 y=2:1599	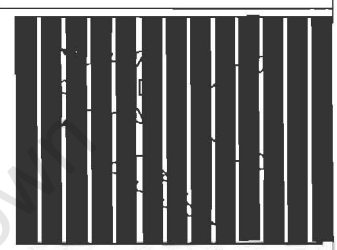
2 – **Square Windowing** x = 402:798 y=402:1198		6 – **Every 6th pixel** x=2:6:1199 y=2:6:1599	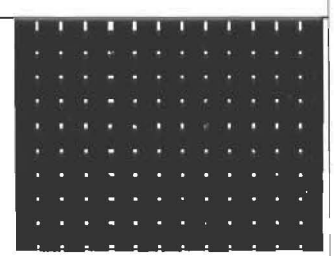
3 – **Rectangular Windowing** x=402:798 y=2:1599	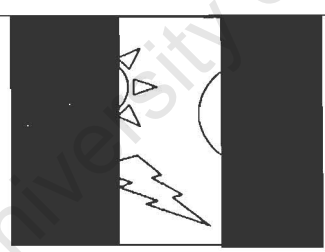	7 – **Every 10th pixel** x=2:10:1199 y=2:10:1599	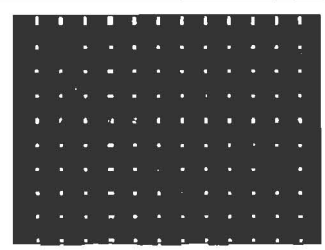

5 AUTOFOCUSING RESULTS

5.1 SLIDE SERIES

As MATLAB cannot communicate directly with the smart microscope, 20 series of images of different slides were used to emulate movement along the z-axis of the microscope. Half of these slide series were obtained from ZN stained sputum smears and all were taken using the smart microscope. It was not deemed necessary to ensure that every slide series contained TB bacilli as a good autofocusing algorithm should be able to focus any slide as long as there is enough image content. The main objects visible in each of the slides were:

- **Slide 1**: Tissue that had been coughed up with the sputum sample
- **Slide 2:** Bacteria (not TB)
- **Slide 3:** Some TB bacilli (stain had faded on this slide due to age and light exposure)
- **Slide 4:** A graduated test slide used to check settings on light microscopes (made by Graticules Ltd., England). The distance between the graduations was 0.01mm.
- **Slide 5:** A blood smear showing red blood cells.
- **Slide 6 - Slide 10:** ZN stained cultured TB slides. These slides were badly stained and bacteria were not easily visible.
- **Slide 11- Slide 20:** ZN stained sputum smears slides. The brown strings of rod shaped objects were *candida* bacteria and other objects such as mucous were also present. (The red stained TB bacteria are not easily seen in the small images in Table 4)

Table 4 The focused slide in each of the slide series.

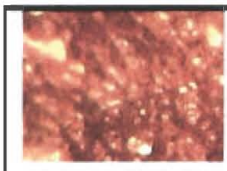			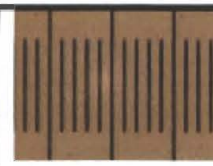	
High Density Slide **Slide 1**	Medium Density Slide **Slide 2**	Low Density Slide **Slide 3**	Test Slide **Slide 4**	Blood Smear Slide **Slide 5**
				
TB Culture **Slide 6**	TB Culture **Slide 7**	TB Culture **Slide 8**	TB Culture **Slide 9**	TB Culture **Slide 10**
				
TB Sputum Smear **Slide 11**	TB Sputum Smear **Slide 12**	TB Sputum Smear **Slide 13**	TB Sputum Smear **Slide 14**	TB Sputum Smear **Slide 15**
				
TB Sputum Smear **Slide 16**	TB Sputum Smear **Slide 17**	TB Sputum Smear **Slide 18**	TB Sputum Smear **Slide 19**	TB Sputum Smear **Slide 20**

5.2 Focus Measure Results

The three focus measures were tested on nine different slide series with differing amounts of image content (high, medium and low), see Table 5. Series containing images of the ZN stained sputum smears were chosen. These are the types of images on which the microscope is required to focus. A focus measure that performs well with these images should be chosen.

Table 5 Focused images from the slide series selected for high, medium and low image content

High Image Content:	Slide Series 1 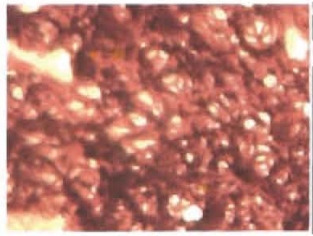	Slide Series 12 	Slide Series 14 
Medium Image Content:	Slide Series 2 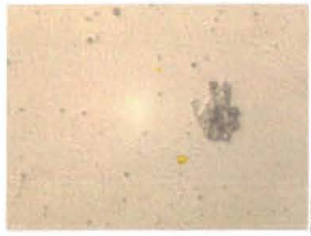	Slide Series 13 	Slide Series 18 
Low Image Content:	Slide Series 3 	Slide Series 16 	Slide Series 20 

The results of the focus measures applied to the slide series are shown in Table 6 (high image content), Table 7 (medium image content) and Table 8 (low image content).

In terms of shape (smoothness and monotonicity) the First Order Gaussian Derivative focus measure plots were the best. However the calculation time for this focus measure was too long for the use of this focus measure to be feasible. The Energy of the Image Laplacian focus measure also displayed an acceptable shape which was very similar to the First Order Gaussian Derivative focus measure although slightly less smooth. The Energy of the Image Laplacian took significantly less computing time than the First Order Gaussian Derivative, thus making it a much more sensible choice.

The Variance of the log-histogram plots have a very poor shape and are not unimodal. Often the maximum value in the Variance of the log-histogram plot corresponded to a slide which was not in optimal focus (see an extreme example - slide series 18 in Table 7). This method consistently underestimated the optimal focus position for slide series with medium and high image content.

These findings resulted in the choice of the Energy of the Image Laplacian as the focus measure to which the search algorithm was applied.

Table 6 Focus measures of high image content slide series

	Slide Series 1	Slide Series 12	Slide Series 14
First Order Gaussian Derivative	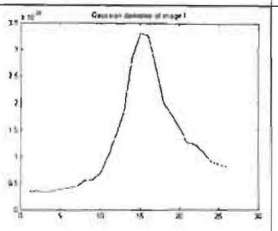	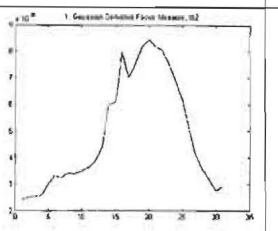	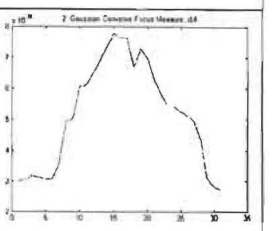
Time taken (s)	3747.3	4465.1	4464.1
Variance of the log-histogram	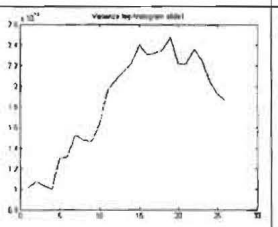		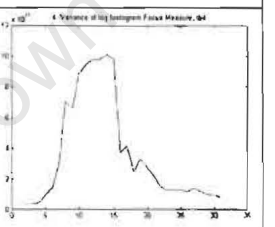
Time taken (s)	28.78	24.04	24.38
Energy of the Image Laplacian	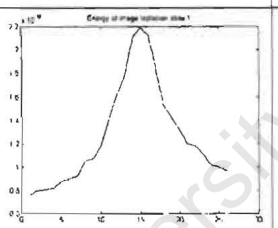	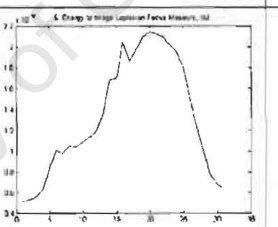	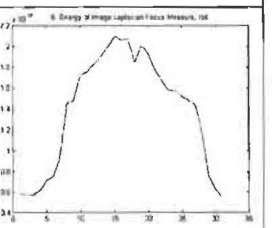
Time taken (s)	24.64	29.18	29.48

Table 7 Focus measures of medium image content slide series

	Slide Series 2	Slide Series 13	Slide Series 18
First Order Gaussian Derivative	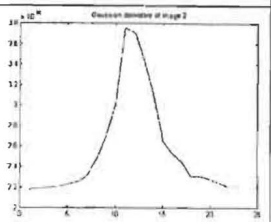	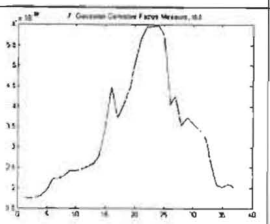	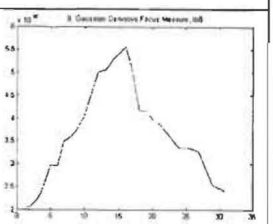
Time taken (s)	3307.8	5323.6	4465.3
Variance of the log-histogram	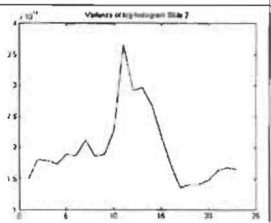	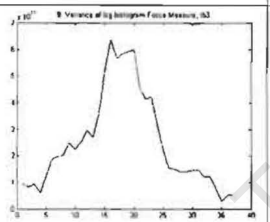	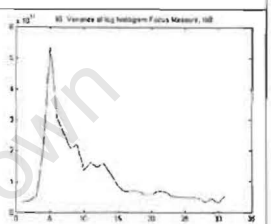
Time taken (s)	21.22	29.02	22.59
Energy of the Image Laplacian	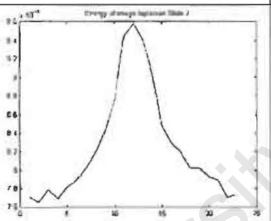	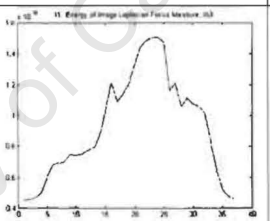	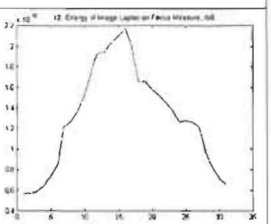
Time taken (s)	21.74	34.86	29.14

Table 8 Focus measures of low image content slide series

	Slide Series 3	Slide Series 16	Slide Series 20
First Order Gaussian Derivative	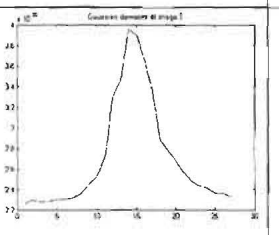	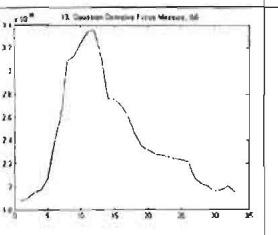	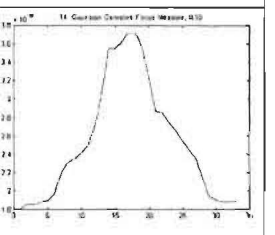
Time taken (s)	3876.2	4749.6	4750.2
Variance of the log-histogram	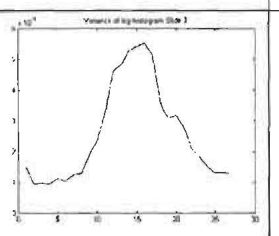	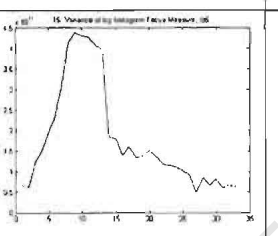	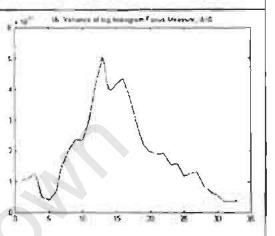
Time taken (s)	23.24	25.47	24.97
Energy of the Image Laplacian	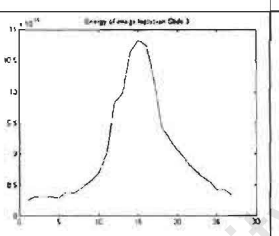	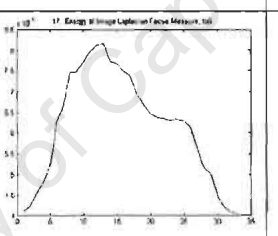	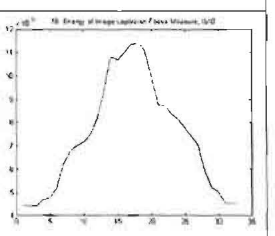
Time taken (s)	25.45	30.99	30.63

5.3 AUTOFOCUSING RESULTS

Whether a slide is in-focus or not is a subjective issue. Geusebroek et al. (2000) compared their autofocusing algorithm against two experienced microscope observers. The maximum error between the two observers was 1.27μm and the between the autofocus method and the observers was 1.12μm. Thus they concluded that their autofocus performance was comparable to experienced observers.

The smart microscope autofocusing algorithm using the Energy of the Image Laplacian focus measure was tested on all 20 different slide series (see Table 4 for the focused image in each of the slide series). The autofocusing algorithm worked well, with each algorithm's position of focus within 4μm of the author's chosen position of focus (see Figure 8).

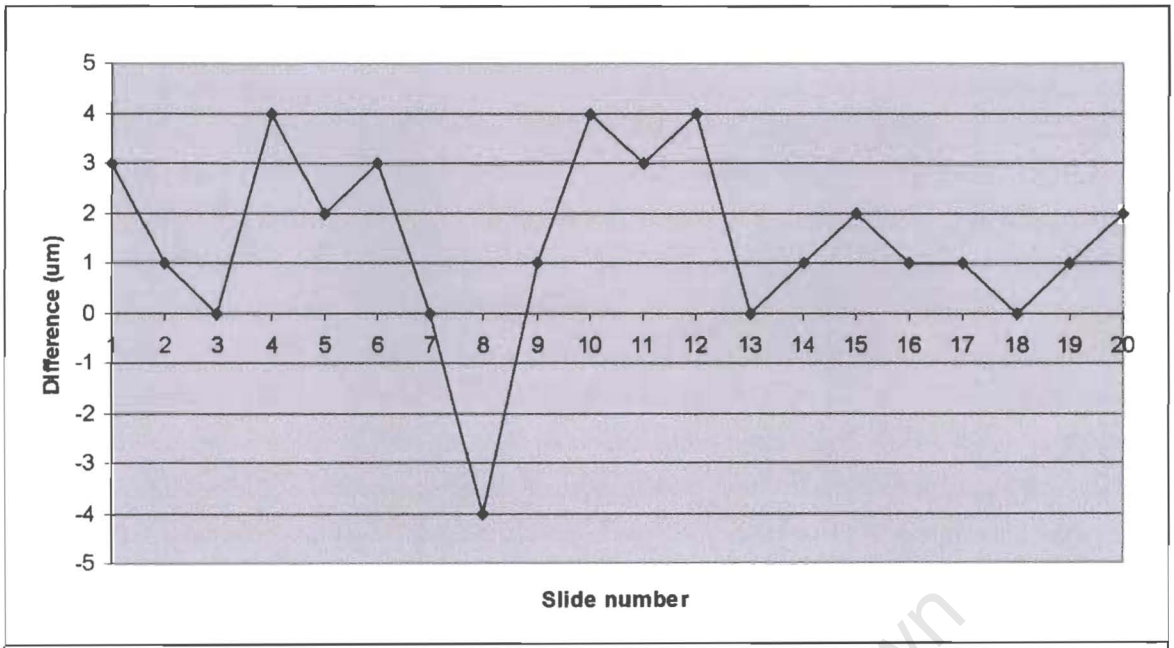

Figure 8 The difference between the autofocusing algorithm's position of focus and the author's position of focus

The average difference between the algorithm's position of focus and the author's was 1.45μm, with a standard deviation of 1.88μm. The average difference was smaller than the depth of focus value for the microscope of 1.6μm (for red light), thus generally both the author's and the algorithms chosen points of focus were considered in focus.

The developed autofocusing algorithm produced good results on 20 test images. The maximum difference between the focal point chosen by the algorithm and that chosen by the author was 4μm. The differences between the focal point chosen by the algorithm and that chosen by the human observer are shown in Figure 9. It was very difficult to decide, by visual inspection, which image was most in-focus. However according to the value of the depth of field (1.6μm) one of these images is out-of-focus as the difference between them exceeds this value.

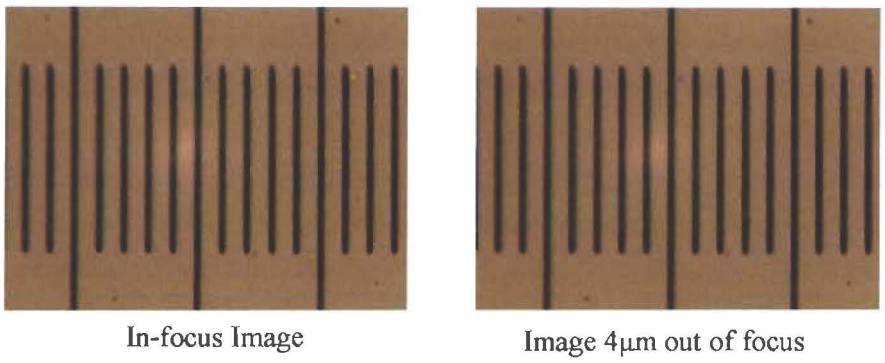

Figure 9 The difference between the focused image chosen by the author (In-focus image) and that chosen by the algorithm

Figure 10 shows how the different amounts of image content affect the differences in the focus position between the autofocusing algorithm and the author. Slides with high image content, have greater differences in focus position. This could be due to the fact that when an image has high image content there is a possibility that the specimen on the slide is thick. In slide series 1, the specimen was a piece of tissue. The tissue was definitely thicker than a sputum smear and this made focussing more difficult. A medium image content slide has the greatest chance of being focussed correctly. When the slide has low image content, the error in the position of focus increases again.

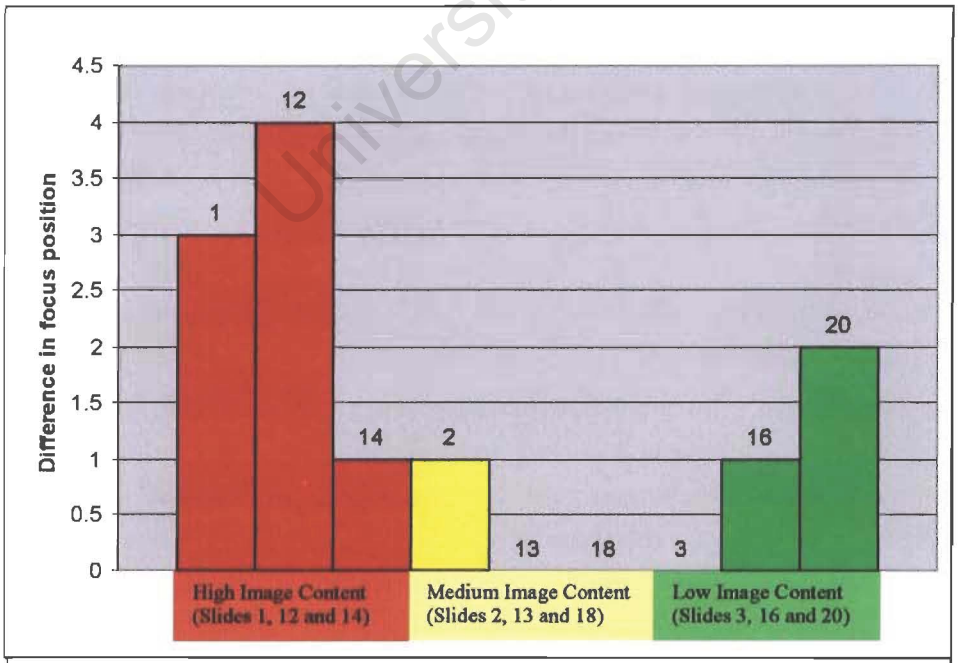

Figure 10 Differences in focussing position between the algorithm and the author for slides with differing image content.

The algorithm developed by Geusebroek et al. (2000) took between 1.5s and 2.8s to focus the microscope. This is in the same time range as experienced microscope observers. This is a considerably shorter time than that taken by the current autofocus algorithm, which took up to 35s to focus. However Geusebroek et al. (2000) used a much smaller image size (780x576) and only every sixth line on each image was processed.

5.3.1 Autofocusing on Adjacent Fields

Variations in slide thickness would result in variations in the position of optimal focus in different fields in the slide thus each field would have to be focused individually. In order to test this variation, a comparison was made between the position of focus for different fields/images obtained from the same slides, for two slides (A and B):

- **Slide A:** Provided slide series 11,12, 18, 19 and 20
- **Slide B**: Provided slide series 13,14, 15,16 and 17

The difference in focus positions between adjacent fields is given in Table 9. Both slides A and B have standard deviations under 10μm thus the amount of time taken to focus adjacent fields after the first field has been focused should be smaller. The standard deviation between the focus positions is an important measure, as the difference in focus positions between fields influences the time taken to process an entire slide.

Table 9 The position of focus for adjacent fields in the same slide

	Number of Slide Series	Position of Focus along z-axis (in μm)
Slide A	11	8287
	12	8272
	18	8279
	19	8281
	20	8292
Average:		**8282.2**
Standard Deviation		**7.66**
Slide B	13	8351
	14	8363
	15	8364
	16	8361
	17	8354
Average		**8358.6**
Standard Deviation		**5.77**

After focusing of the first field in the slide has occurred, direct communication between the focusing software and the software controlling the position of the z-axis, would allow the time taken to focus adjacent fields to be tested.

The results of emulating the focusing of adjacent fields after focusing of the first field are shown in Table 10. The time taken for each slide series when run from a small distance from the position of optimal focus is shown.

Table 10 Showing the time taken when fields in slides A and B are focused from a small distance away from the optimal focus position

	Slide Series	Distance away from position of optimal focus (μm)	Time Taken (s)
Slide A	11	12	11.64
	12	22	13.22
	18	21	14.99
	19	19	15.02
	20	17	12.34
Slide B	13	1	10.60
	14	12	15.93
	15	14	11.43
	16	11	11.47
	17	29	14.16

As used with slide series 13 in the table above, the smallest distance away from the position of optimal focus was 1μm. The time taken to move the 1μm to the position of focus was 10s. This indicated that the shortest time possible could be limited to about 10s. Only the translation of the code from MATLAB to C++, and the acquisition of a faster processor, will bring the time required to focus adjacent fields to under 10s. It should also be noted that the times in Table 10 do not take into account the time required for mechanical movement of the microscope stage while searching for the position of optimal focus.

5.3.2 Windowing Results

The seven windowing methods were applied to the first 10 slide series in an attempt to reduce the amount of time it took to achieve the focused position, see Table 11. It must be noted that each time an image in the slide series was processed, it had to be loaded by MATLAB. This increased the time taken for the autofocusing. Once the algorithm is converted to C++ and can communicate directly with the microscope and camera, the processing time taken to obtain the focus position should decrease.

The average amount of time taken to focus the original, full-sized slide images was 20.59s

Table 11 The windowing methods, the average time taken by each method and the number of seconds faster than the original average time.

Windowing Method Number	Avg. Time taken (s)	Time faster than original average (s)
1	18.55	2.04
2	18.03	2.55
3	18.75	1.84
4	18.02	2.57
5	18.62	1.97
6	17.66	2.93
7	17.05	3.54

The different windowing methods decreased the time taken by up to 3.5s and when it worked, it worked well. However when it failed, it failed catastrophically. The incorrect direction in the difference-of-signs method was chosen five times during windowing. This never occurred when windowing was not used. An incorrect direction in the difference-of-signs means that the microscope will never be able to focus the image.

5.4 AUTOFOCUSING DISCUSSION

5.4.1 Focus Measures

The results of the focus measure experiments showed that the Energy of the Image Laplacian was the best choice for use in the autofocusing algorithm. Even though the First Order Gaussian Derivative focus measure provided excellent results, the long time it took to process was undesirable. The Energy of the Image Laplacian focus measure was nearly identical in shape to the First Order Gaussian Derivative focus measure, but it took a considerably shorter time to run. The fact that the autofocusing algorithm performed well is proof that the Energy of the Image Laplacian was a good choice for a focus measure.

5.4.2 Autofocusing Algorithm

The developed algorithm worked well although there was a maximum discrepancy of 4μm between the position of focus found by the author and that found by the algorithm. This discrepancy was larger than the depth of field. However the average difference was smaller than the depth of field value (1.6μm) for the microscope. If the author's performance is regarded as the gold standard, the algorithm's chosen points of focus can be generally considered acceptable.

The effectiveness of the algorithm has been demonstrated on 20 slide series. Slides that contained too much image content or not enough, had higher discrepancies in the difference of the focus

position between the autofocusing algorithm and the author. The time taken to autofocus the microscope was ±10x longer than the time reported by Geusebroek et al. (2000). One of the reasons for this discrepancy was that the image size used by Geusebroek et al. (2000) was 780x576 pixels which was over 4 times smaller than the images from the smart microscope, and only every sixth line was processed. A smaller image allows for a much faster processing time.

Adjacent fields in the same slide had a standard deviation of 6 to 8µm. The focusing time from field to field would thus be less than focusing from a position completely out of focus. Once the algorithm is translated into C++ and a faster processor is acquired the time taken to autofocus adjacent fields will probably fall below 10s. However, the time taken for the microscope stage to move during focusing when the focusing algorithm is integrated with the microscope control software, would add to focusing time.

5.4.3 Windowing

Windowing the image before finding its focus measure saved up to 3.5s in the time taken to run the autofocusing algorithm. However windowing also caused the algorithm to fail. This occurred whenever the window was chosen such that vital information in the image was not selected. The time saved by windowing is not worth the chance of autofocusing failure. Thus it was decided not to use windowing in the final algorithm.

5.5 AUTOFOCUSING CONCLUSION

An autofocusing algorithm has been developed and tested for the smart microscope. The algorithm worked satisfactorily for all of the slide series on which it was tested, but it did run more slowly than autofocusing algorithms reported in the literature. The algorithm developed here used the Energy of the Image Laplacian focus measure and did not use windowing.

6 LITERATURE REVIEW OF IMAGE SEGMENTATION FOR BACILLUS DETECTION

6.1 INTRODUCTION TO SEGMENTATION

Image segmentation is one of the most critical and difficult steps in image analysis and pattern recognition. It has been studied extensively over the years, but there is still no definitive solution for each imaging problem. Good image segmentation can make or break a pattern recognition or analysis system. In all areas of use the quality of the final output depends largely on the quality of the segmentation output (Pal and Pal, 1993).

Image segmentation is the process of partitioning the image into non-intersecting regions such that each region is homogenous and the union of no two adjacent areas is homogenous (Pal and Pal, 1993) i.e. the separation of objects in the image from each other and the background. However the problem of image segmentation is also one of psychophysical perception and is therefore not readily solved by purely analytical techniques (Fu and Mui, 1981). The ultimate goal of image segmentation is to identify which part of an array made up of numbers represents an object in the real world (Olabarriaga and Smeulders, 2001). Currently a human being is the best judge of segmentation results (Pal and Pal, 1993).

Image segmentation can be performed on grey-scale or colour images and has been classified into a number of different approaches by different authors. According to Pal and Pal (1993) there are hundreds of segmentation techniques available in the literature. No single technique will ever work well for all types of images. The selection of an appropriate technique for a specific type of image is a difficult problem. Pal and Pal (1993) classified the image segmentation methods they reviewed into 6 different methods whereas Fan et. al. (2001) classified image segmentation methods into four basic techniques. Their classification methods are summarised as follows:

1) **Thresholding techniques:** These techniques are widely used and tend to be simple to implement. Thresholding assumes that adjacent pixels whose values lie within a certain range belong to the same object. Good segmentation can be obtained when the image contains only two principal components. Thresholding techniques ignore any spatial information contained in the image. Thresholding can be performed globally (over the whole image) or locally (image partitioned into several sub regions each with its own threshold). Thresholding can also be classified as bi-level or multilevel thresholding. Bi-level thresholding is equivalent to classifying the image into two classes: object and background. Multilevel thresholding is used when the image is composed of several objects with different surface characteristics.

2) **Boundary-based techniques:** These techniques assume that there is a rapid change in pixel values at the boundary between two regions in an image. Edge detectors such as Sobel, Roberts and Canny fall into this category. Boundary-based procedures can require post-procedures such as gap filling and smoothing, which can be time-consuming.
3) **Region-based techniques:** These rely on the assumption that adjacent pixels in the same region have similar properties such as colour, grey level or texture. Seeded region growing is a common technique in this category.
4) **Hybrid techniques:** These techniques combine boundary detection and region growing. They are the one of the newest forms of image segmentation.
5) **Segmentation of colour images**: Transformations into different colour spaces can help to segment the image. Spectrum analysis can be used, in which prior knowledge about the colour of the objects in the image is used to aid in the segmentation. A colour image can be regarded as a special case of a multispectral image and thus algorithms developed for grey-scale images can be used.

6.1.1 Image Segmentation of Tuberculosis Bacilli

According to Forero et. al. (2004) the segmentation of any specific type of bacteria is a complex problem. The bacillus shape does not provide enough information to be used as a discriminant feature as other bacteria species may share the same shape. Thus the colour information provided by the staining of the bacteria should be an essential part of the segmentation process. Only a preliminary study has been performed on TB bacilli stained with ZN stain, whereas a number of studies have been published on TB bacilli stained with fluoroscope auramine.

The preliminary study on the automatic detection of TB in ZN stained sputum smears was done by Veropoulos (1998). The following method was used:

1) **Data preparation and image capture**: ZN stained sputum smears were used with a light microscope. Images were captured using a digital camera attached to the microscope with a magnification of x630.
2) **Image processing and analysis**: Images were converted from colour RGB images to HSI images. The grey-scale image from the saturation band was used. The image was segmented by thresholding using its average intensity value. Edge detection using a Canny operator was applied and then each region was labelled and tested for size. If the region was too large to be a bacillus it was removed. Edge-pixel linking and boundary tracing were then used to ensure the regions had closed borders and that each region was outlined. Shape descriptors were then found from each region and its boundary. These shape descriptors were necessary for the recognition of each object.

3) **Image recognition**: The shape descriptors and the average RGB values found from the objects were fed into a classifier to identify any relevant regions as bacilli. A number of classification techniques were used to identify the bacteria. The approach that performed best in terms of overall accuracy was a multi-layered neural network with one hidden layer, trained by using standard back-propagation.

Veropoulos et al. (1998) used shape descriptors and neural networks to segment the fluorescent TB bacilli. No colour information was used in their method, which consisted of the following three steps:

1) **Data preparation and image capture**: Auramine stained sputum smears were used with a fluorescent microscope. Images were captured using a digital camera attached to the microscope with a magnification of x630.
2) **Image processing and analysis**: Edge detection using a Canny operator was applied to the TB images. Each region was then labelled and tested for size. If the region was too large to be a bacillus it was removed. Edge-pixel linking and boundary tracing were then used to ensure the regions had closed borders and that each region was outlined. Shape descriptors can then be found from each region and its boundary. These shape descriptors are necessary for the recognition of each object.
3) **Image recognition**: The shape descriptors found from the objects were fed into a classifier to identify any relevant regions as bacilli. A number of classification techniques were used to identify the bacteria. The approach that performed best in terms of overall accuracy was a multi-layered neural network with one hidden layer, trained by using standard back-propagation.

Forero et al. (2004) used Canny edge detection and morphological operators followed by adaptive colour thresholding.

1) **Data preparation and image capture**: Forero et al. (2004) used a medium magnification of x 250 to capture their images of the auramine stained bacteria. The TB bacilli fluoresce in a range of green-yellow to white.
2) **Image processing and analysis:** The image segmentation was performed using a Canny operator. Morphological operators such as opening were applied to ensure that regions that are too small to be bacteria are deleted. From observations of the image histograms Forero et al. (2004) concluded that all the bacilli showed up very strongly in the green channel. An adaptable colour threshold was applied to the green channel with the threshold defined as a weighted difference between the maximum and average luminance values obtained from the green channel. Thus once the image is segmented only the objects that have the same bacilli colour are retained.

3) **Image recognition**: By means of a visual inspection of the bacilli, Forero et al. (2004) decided that because the bacilli do not have a uniform shape, a better representation of the bacilli can be made by subdividing them into several clusters according to their shape, thickness and length. Different feature descriptors for the bacteria were also evaluated. Several different clustering algorithms were tested, with the *k-means* clustering algorithm being preferred because of its simplicity.

6.2 Grey Scale Image Segmentation

As discussed above, one of the most common forms of grey-scale image segmentation is grey-level thresholding. Successful segmentation of objects in a grey-scale image should take into account both the grey-level values and the object shape (Erikson, 2006). Grey-scale image segmentation seemed appropriate for the segmentation of the TB bacilli out of the image from the microscope, as it is easy to implement and intuitively seems possible. In the colour image, the TB bacteria are red and opaque against a light blue background. Thus the intensity of the background and the bacteria should be different and it should then be possible to find a threshold that will segment the bacteria from the background in a grey-scale image. Object shape was not considered as it was beyond the scope of this thesis.

There are two major forms of grey-scale thresholding: crisp and fuzzy.

6.2.1 Crisp Thresholding

Crisp thresholding involves finding a critical value or threshold in the histogram of an image (Tobias and Seara, 2002). When this threshold is applied to an image, pixels with grey level values that exceed the threshold are assigned to one set (for example the object set) and the rest are assigned to another set (for example the background set). In a well defined image the histogram will have two peaks separated by a deep valley (this is known as a bimodal histogram). One of these peaks would represent the background and the other the object. Thus to segment the image the threshold would be located somewhere in the valley. There are a large number of algorithms developed to find this threshold. Some algorithms use an iterative scheme to separate the pixels others rely on entropy (either trying to minimise the spatial entropy of the image (Brink, 1995) or using the entropy (a measure of the randomness) of the histogram to find the threshold (Kapur et al., 1985)). In general, most histogram based thresholding algorithms work very well when the histogram is bimodal or nearly bimodal.

However, these algorithms will fail to perform when the histogram is unimodal (one peak) or multimodal (multiple peaks). This will occur whenever an image is ill defined or corrupted by

noise or bad illumination. In these cases, as there are no clear distinctions between the objects and the background, fuzzy thresholding is recommended.

6.2.2 Fuzzy Thresholding

Thresholding a unimodal or multimodal histogram cannot be performed by using normal set theory. To quantify the similarity between grey levels, fuzzy set theory must be used. Pal et al. (1983) computed a global fuzzy measure for every possible grey level in the image. The optimum threshold was found by minimising the measure. For bimodal histograms this approach works well, however for irregular histograms a minimum may not be found in the measure (Tobias & Seara, 2002). Another method proposed by Tobias and Seara (2002) does not involve the minimization of a criterion function, instead the histogram is thresholded based on the criterion of similarity between the grey levels.

6.2.3 Basic Fuzzy Set Theory

A fuzzy set is a class of points possessing a continuum of membership grades where there is no sharp boundary among elements that belong to this class and those that do not (Zadeh, 1965).

Let each point (x_i) in set A have a characteristic function $\mu_A(x_i)$. This function assigns to each member of the set a degree of membership in the range [0,1].

A number of different characteristic functions for membership exist. The S-function (see Figure 11) is commonly used (Jantzen, 2004).

$$\mu_{As}(x) = S(x_l, x_r, x)$$

$$= \begin{cases} 0 & x < x_l \\ \frac{1}{2} + \frac{1}{2}\cos((x-x_r/\, x_r-x_l)\pi) & x_l \le x \le x_r \\ 1 & x \ge x_r \end{cases}$$

where x_l is the left-most point of the S-function

x_r is the right-most point of the S-function

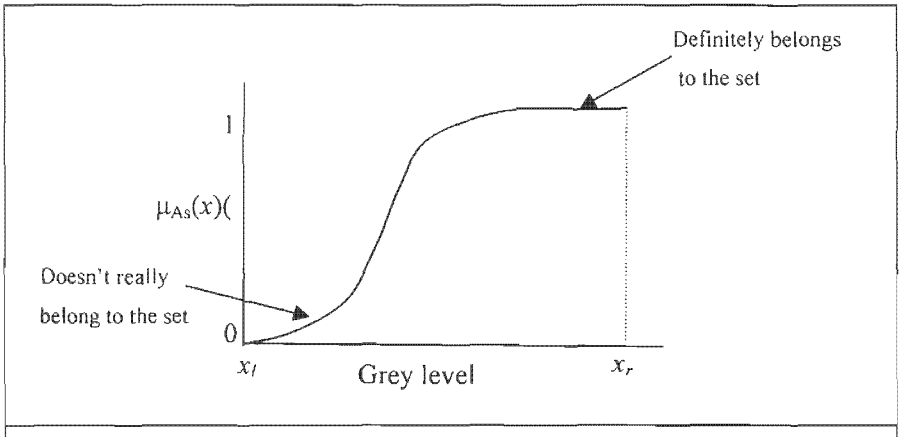

Figure 11 An example of an S-function

For an MxN image with L grey levels, g Є [0, L-1], the histogram h(g) and the membership function $\mu_A(g)$ the linear index of fuzziness (γ) can be found as follows (Tizhoosh, 2005)

$$\gamma_l(A) = \frac{2}{MN} \sum_{g=0}^{L-1} h(g) \times min[\mu_A(g), 1 - \mu_A(g)]$$

This linear index of fuzziness gives an indication of how well a certain element value fits into a set of other elements. If the γ of a set is low, it means that the objects in the set are very similar. In a thresholding segmentation situation with sets (e.g. Object1, Object2 and Background) each grey value in the image should be assigned to the set which has the lowest γ when that grey value is a member of it.

6.2.4 Conclusion on Grey Scale Image Segmentation by Thresholding

Thresholding is a readily implemented technique to segment images and is the simplest and most popular strategy for segmentation. Classical crisp thresholding is associated with loss of structural information in the image, however fuzzy thresholding preserves the identities of pixels (Jawahar et al., 2000). The main problem with grey-scale image segmentation in general is that no colour information is taken into account. The two factors that make the TB bacteria distinguishable are shape and colour. Although shape information could be used this is not easily done and was beyond the scope of this thesis.

6.3 Colour Image Segmentation

Colour image segmentation is currently a growing field of research. As computing power increases, so colour image processing becomes easier and more feasible to perform. Most current colour image segmentation algorithms are extensions of the grey-scale algorithms. A colour

image can be considered to be an overlay of monochrome digital images, each layer representing one of the primary colours (Castleman, 1998). Viewing colour images in this manner allows a grey-scale image segmentation algorithm to be applied to each layer of the image.

6.4 COLOUR SPACES

There are a number of different ways to specify colour in an image. Colour is perceived by humans as a mix of the three primary colours red, green and blue. This is mimicked in the colour space known as RGB. From this colour space other colour spaces can be derived by using linear or non-linear transformations. Selecting the best colour space for an application is still one of the difficulties in colour image segmentation (Cheng et al., 2001).

6.4.1 RGB Colour Space

RGB is the most commonly used colour space. It is used for television (TV) display and for pictures acquired by digital cameras. RGB is based on the fact that any colour can be made up by using a specific combination of the three colours. It can be represented geometrically by a 3-d cube, where the coordinates inside the cube represent the values of red, green and blue respectively (see Figure 12).

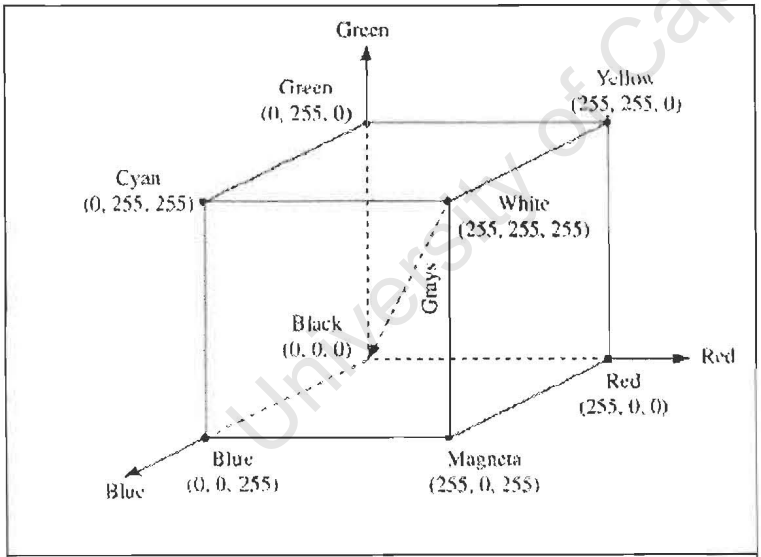

Figure 12 The RGB colour cube (Cheng et al., 2001)

The RGB colour space obeys the laws of colourimetry (Cheng et al., 2001):

1) Any colour can be created by these three colours and any combination of the three colours is unique.
2) If two colours are equivalent, they will again be equivalent after multiplying or dividing the three components by the same number

3) The luminance of a mixture of colours is equal to the sum of the luminance of each colour.

RGB is good for colour display but is not seen as useful for colour image segmentation as there is high correlation between the R, G and B components. This means that if the intensity changes, all three components will change accordingly (Cheng et al., 2001).

6.4.2 HSI (Hue-Saturation-Intensity) Colour Space

HSI colour space is another common colour space. It is based on the way in which humans perceive colour. The HSI system separates the colour information from the intensity information. Colour information is given in the hue and saturation values while intensity describes the brightness or amount of light in the image. HSI can be explained in the following way:

- Hue: This represents the basic colour
- Saturation: This describes the purity of the colour
- Intensity: This is the brightness of the colour

HSI can be represented geometrically in the following way. Hue is considered as an angle between a reference line and the colour point in RGB space. Saturation is represented by the radial distance to the centre of the cylinder and intensity is the height in the axis direction (Cheng et al., 2001), see Figure 13.

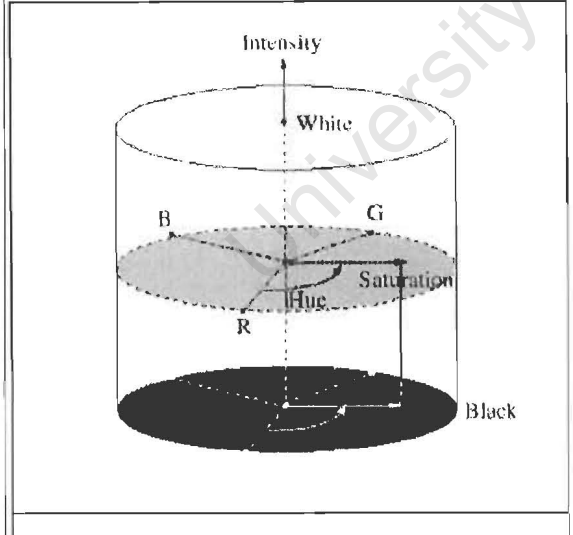

Figure 13 HSI Colour Space (Cheng et al., 2001)

HSI space is particularly useful when trying to segment images that have non-uniform illumination, as hue is only dependent on the intensity values. However hue has a non-removable

singularity near the axis of the colour cylinder and this can cause discontinuities in the representation of colours (Cheng et al., 2001).

6.4.3 YUV Colour Space

YUV is a type of television colour representation for use in European countries. It is formed through a linear transformation of RGB coordinates. Luminance is stored in the Y value and the U and V contain information on the chrominance. U contains the difference between the blue component and a reference value and V contains the difference between the red component and a reference value (MATLAB, 2002).

6.5 Segmentation Methods

A number of colour segmentation methods exist, however the literature on colour segmentation is not nearly as extensive as that on grey-scale image segmentation (Cheng et al., 2001). Most grey-level image segmentation techniques can be extended for use with colour images, however one of the problems is how to employ the colour information as a whole for each pixel. When the colour is projected into its three components the colour image becomes a multispectral image and the colour information that humans can perceive is lost. The different colour segmentation techniques reviewed are colour edge extraction (Fan et al., 2001) and Canny edge detection (Ihlow and Seiffert, 2003).

The colour edge extraction technique was chosen because of the excellent segmentation results Fan et al. (2001) achieved in their research. Their application was the segmentation of a human face from a background in colour images. Their edge extraction algorithm worked better (provided more accurate edges) than the standard Prewitt, Sobel, Laplacian and Roberts operators which they also tested on their images.

The Canny edge detection technique (Ihlow and Seiffernt, 2003) was chosen because it has been used to segment blue-green dyed barley cells (see Figure 14) from a yellow-green background in microscope colour images is an application very similar to the segmentation of TB bacteria from microscope colour images.

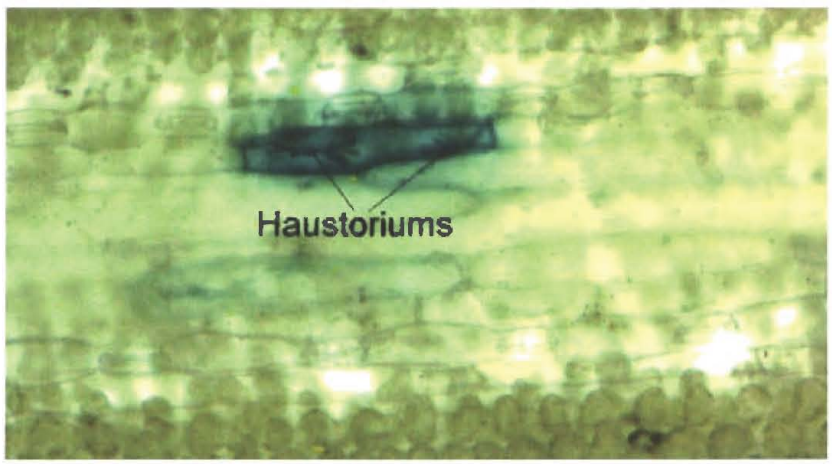

Figure 14 Image taken from Ihlow and Seiffert (2003) showing dyed genetically altered barley cells (Haustoriums are sections containing powdery mildew)

6.5.1 Colour Edge Extraction

Fan et al. (2001) developed a boundary-based technique which uses an isotropic (invariant with respect to direction) colour-edge detector and entropic thresholding (the entropy of the edge detected pixels added to the non-edge pixels is maximised at the optimal threshold point). The colour space used is the YUV colour space and it was selected because the chrominance is explicitly separated from the luminance.

An edge in a digital colour image can be defined as two adjacent pixels that differ significantly in brightness or colour. Both changes in brightness and colour should be exploited for efficient edge detection.

The algorithm developed by Fan et al., (2001) uses a second-order neighbourhood to describe the relationship between pixels (see Figure 15). An edge may pass through the second-order neighbourhood of a pixel in one of four directions, namely horizontal (HOE), vertical (VOE), northeast diagonal (NOE) and northwest diagonal (SOE). These edge strengths are calculated as a weighted sum of the pixel values, see Figure 15 for the weight coefficients.

The local maximum edge strength of a pixel is the maximum of the four edge strengths.

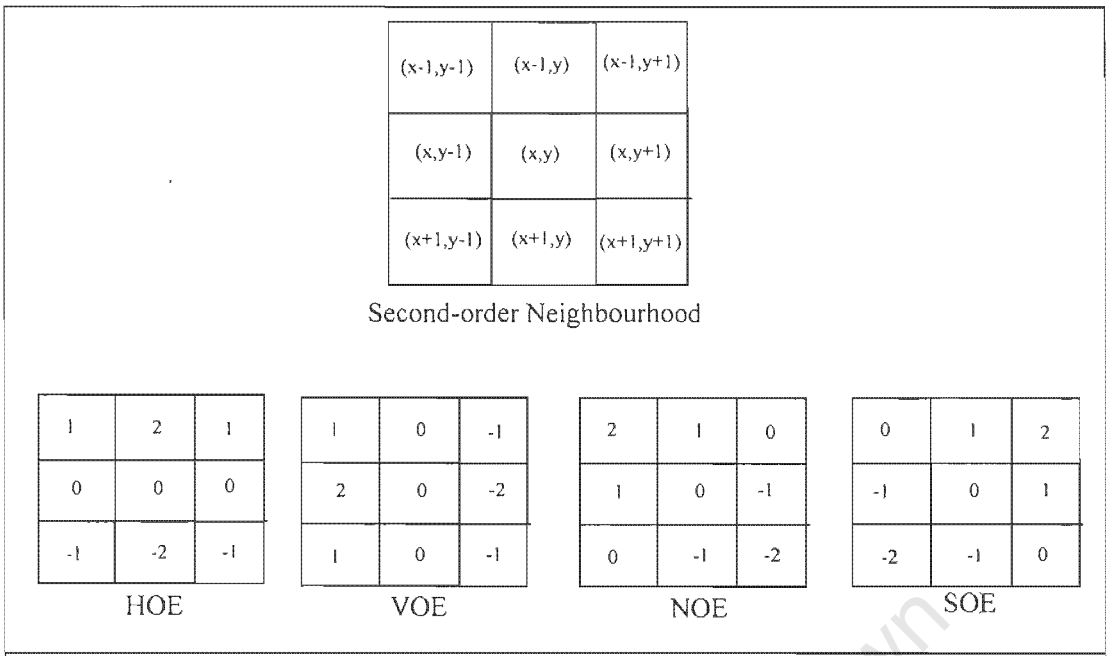

Figure 15 Second-order neighbourhood and pixel weighting to calculate edge strengths.

The next step is to classify the pixels in the luminance component as either edge or non-edge. This is done by comparing the local maximum edge strength of the pixel to an optimum threshold. The optimum threshold is found using an entropic thresholding technique which involves finding the minimum for a criterion function which relies on the entropies of the edge and non-edge pixels.

An analogous edge detection procedure is carried out on the U and V chrominance components. The edge results for the three components are then integrated through the following rule: pixel (x,y) is classified as an edge pixel if one of its three colour components classifies it as an edge pixel.

Fan et al. (2001) tested this algorithm against a variety of other isotropic edge detectors. The results showed that the algorithm provided more potential edges than other edge detectors in the same conditions.

6.5.2 Canny Edge Detection

Ihlow and Seiffert, (2003) addressed the problem of detecting and segmenting stained genetically modified barley cells from unmodified cells in colour microscope images. Two techniques were investigated:

1) **Segmentation by pixel-colour classification**: This is based on an extension of grey level histogram thresholding. Because each colour pixel is not a scalar value but a vector (generally consisting of RGB components) a multivariate Gaussian model approach was used. This method uses the information found from a colour histogram (generated from the image) to make a parametric model which can be used for statistical decision making. Results of this method show that this technique suffers from a lack of spatial information. Images with strongly coloured cells can be labelled correctly but any weakly coloured cells are detected as fragmented regions. Since training data are needed for this classification technique, variations in the data concerning luminance and colour parameters will only degrade the segmentation results. No information is given on how representative the training data is, and how much the training data resembles the non-target objects.
2) **Segmentation by edge detection**: This technique exploits spatial information to find salient features in the image. The Canny edge detector is one of the most powerful edge detectors developed. It is so useful because it detects both strong and weak edges in the image and includes the weak edge in the final product only if it is connected to a strong edge (MATLAB, 2002). Ihlow and Seiffert (2003) found that when the Canny edge detector is applied to the image in the RGB colour space, the edge detector highlighted unwanted parts of the image. Thus they transformed the image into HSV (Hue-Saturation-Value equivalent to HSI) colour space and then applied the Canny edge detector to the Hue channel. Results of this method were very promising. The object boundaries were clearly detected and outlined.

6.5.3 Colour Compensation

Colour compensation is a technique that was developed for fluorescence microscopy. It is used in a technique called Fluorescence In Situ Hybridization (FISH) which uses multiple DNA probes, each tagged with a different fluorophore, to visualise several different cellular structures simultaneously. This allows several different molecular components to be visualised in different colours (Castleman, 1994).

Different fluorophores and stains have different, often broad, emission and absorption spectrums. Commonly used colour cameras also have broad and overlapping sensitivity spectra. Given the

overlap of the emission spectra it is very difficult to design a system so that each fluorophore only appears in one colour channel. Even using a monochrome camera and carefully selected fluorophores and colour filters, spectral overlap still spreads each fluorophore across the colour channels to some extent (Castleman, 1994). When using a colour CCD camera the situation is even worse.

Colour compensation was developed to isolate each fluorophore to a single channel. It is an image processing technique that operates on a digital image immediately after the image is acquired. For an N-colour system, an NxN matrix is required to perform colour compensation. This matrix is determined experimentally for a particular combination of fluorescent dyes, filters and camera (Castleman, 1993). The concept behind colour compensation is that the brightness of the red fluorophore (for a three-colour RGB system) is spread among the three channels (R, G and B) by the imaging process and likewise for the green and blue dyes.

The matrix C that specifies the spreading of the colour in each channel is determined experimentally (Castleman, 1993). Each element in C is the proportion of the brightness from the fluorophore that makes its way into each channel.

If A is the 1x3 vector of true fluorophore brightness values, then B = A x C is the 1x3 vector of RGB grey levels as recorded by the camera.

Let **D** denote a 3x3 compensation matrix such that:

$$\mathbf{B} \times \mathbf{D} = \mathbf{A} \tag{1}$$

This means that $\mathbf{C} * \mathbf{D} = \mathbf{I}$ (3x3 Identity matrix). This can be satisfied if

$$\mathbf{D} = \mathbf{C}^{-1} \tag{2}$$

Thus equation (1) becomes

$$\mathbf{A} = \mathbf{B} \times \mathbf{C}^{-1} \tag{3}$$

The inverse of the colour spread matrix, called the 'colour compensation matrix', specifies what must be done to correct the colour spread.

Colour spread compensation can eliminate colour spreading and can be used for any number of colour channels and fluorophores. However, it cannot be used when the number of fluorophores exceeds the number of colour channels.

Colour spread compensation is a useful technique as it separates out the colours in the image and relegates each of them to their respective colour band. Although this technique has never been used on images from a light microscope it might be very useful in the task of separating the red coloured TB bacteria from the blue coloured background. As the bacteria are the only red objects in the image, they should be assigned by this method to a colour channel of their own. A segmentation algorithm could be applied to this colour channel and only the bacteria would be detected.

6.5.4 Artificial Neural Networks

ZN staining colours TB bacilli red, however any other *myobacterium* present will also pick up the red stain. Any mucous present on the slide will also stain red, thus eliminating the blue background. Technologists, when faced with mucous on a sputum slide, will only focus fields where the mucous is not present, as any definition between the TB bacilli and the background is lost. Thus the identification of TB bacilli based on colour alone is not sufficient. Other techniques such as artificial neural networks (ANNs) and classification should be used to ensure that the segmented objects really are TB bacilli.

A neural network can be defined as a mathematical algorithm that is comprised of interconnected simple and adaptive processing elements (artificial neurons or nodes) that are capable of performing massively parallel computations for data processing and knowledge representation (Basheer and Hajmeer, 2000). Figure 16 shows the basic structure of a neural network. There are normally three types of layers within an ANN: the input layer collects the information, the hidden layer provides extra processing capabilities and the output layer generates the response to a given input (Papik et al., 1998). Artificial neural networks have many applications in microbiology such as:

- Pattern recognition of DNA
- Prediction of microbial growth
- Identification of micro organisms and molecules.

ANNs have the ability to learn, where learning is viewed as the process of updating the internal response of the structure to external stimuli so that it can perform a specific task. ANN learning is performed iteratively as the network is given training examples (Basheer and Hajmeer, 2000). It is important to note that neural networks do not classify data exactly, but rather give a measure of resemblance between an actual input pattern and the example patterns taught earlier to the network (Wit and Busscher, 1998).

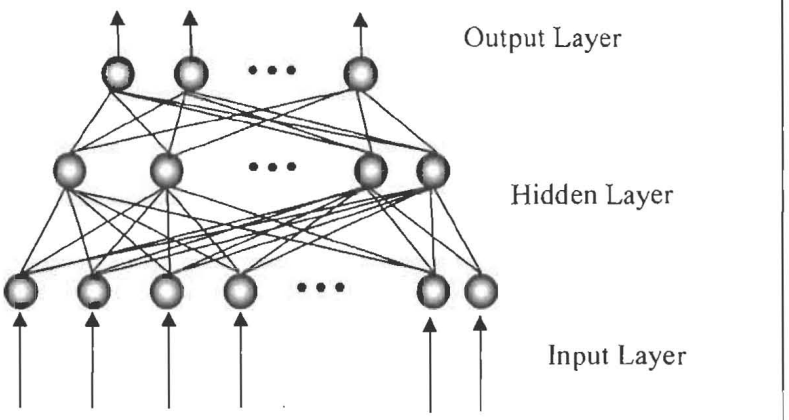

Figure 16 Neural network basic structure (Papik et al., 1998)

Artificial neural networks can be classified in a number of different ways, according to one or more of their relevant features. The most common classification of ANNs is based on the following (Basheer and Hajmeer, 2000):

- The function the ANN is designed to perform (e.g. clustering, pattern association, modelling, prediction etc.)
- The degree of connectivity of the neurons in the network
- The direction of the flow of information in the network
- The type of learning algorithm used to train the ANN
- The amount of supervision the ANN requires during training.

Wit and Busscher (1998) used neural networks to detect and count bacteria and yeast adhering to solid structures. They bypassed the use of any image segmentation process and applied the ANN directly to the image. A feed-forward ANN was used that processed a 9x9 grey-scale sub-image taken sequentially from the main image. An accuracy of 93-98% was achieved in the enumeration of the bacteria and an accuracy of 98% in the enumeration of yeast cells.

6.5.5 Classification

Classification or clustering is the partitioning of data into subsets, so that the data in each subset share a common feature. A large number of clustering algorithms are available in the literature such as k-means clustering and fuzzy c-means clustering. ANNs can also be used to classify data.

Veropoulos et al. (1998) used a Canny operator to perform edge detection on their TB images. Shape descriptors were then found from the segmented objects and fed a multi-layered neural network with one hidden layer, trained by using standard back-propagation.

Forero et al. (2004) used a colour thresholding method to segment possible bacteria from the image. Feature descriptors were then obtained from the shape of the segmented objects and k-means clustering was used to classify the objects into TB bacteria and non-bacteria sets.

6.6 Conclusion to Segmentation

Segmentation is a critical step in the detection of bacteria in microscopy images. A large number of segmentation methods exist and many of them give different results when applied to the same image. Thus the difficulty is in deciding which segmentation algorithm gives the best results for a certain application.

In this thesis the optimum result from the segmentation process would be the separation of the TB bacilli from the rest of the image. However, the stained colour of the TB bacilli might not be unique enough to rely purely on colour segmentation for bacillus detection. The use of ANNs or other classification methods to decide whether segmented objects are TB bacilli was beyond the scope of this thesis.

7 SEGMENTATION METHODS

In this chapter the segmentation experiments that were performed on images from the smart microscope and from the conventional microscope are described in detail.

7.1 GREYSCALE SEGMENTATION

Two forms of grey-scale segmentation were investigated. Crisp and fuzzy thresholding were chosen because they are easy to implement and can quickly give an idea if the bacteria can be segmented from the image without any colour or shape information being used.

7.1.1 Crisp Thresholding

To perform crisp thresholding on images obtained from the microscope the following procedure was followed:

1. The chosen image was read into the MATLAB programming environment using the `'imread'` command.
2. The image was converted from a colour RGB image to a grey-scale image using the `'rgb2gray'` command.
3. The histogram of the image was then found and shown using the `'imhist'` command. The user then decides on a grey value threshold.
4. A matrix filled with zeros that is the same size as the image was created.
5. A `'for'` loop was used to run though every pixel in the image. If the grey level value of the pixel was higher than the threshold value then the element in the zero matrix at the corresponding position of that pixel was set to '1'.
6. The command `'bwperim'` was used to display the outline of the binary thresholded image on top of the original grey-scale image.

7.1.2 Fuzzy Thresholding

To perform fuzzy thresholding the following algorithm adapted from Tobias and Seara (2002) was used:

1. The chosen image was read into the MATLAB programming environment using the `'imread'` command and converted from RGB to greyscale using the`'rgb2gray'` command.
2. The equalised histogram of the image was calculated using the `'histeq'` command.
3. The normalisation factor α was calculated. This factor normalises the index of fuzziness for both the Background and Object sets, thus allowing them to be compared. α was computed as follows:

- The fuzzy subsets of Object and Background were modelled by two fuzzy subsets of the grey level set **X**. The Object set was associated with the interval $[x_{min}, x_j]$ and the Background set with $[x_r, x_{max}]$, where x_j and x_r are the final and initial grey values for these subsets and x_{min} and x_{max} are the lowest and highest grey levels of the image respectively. x_j and x_r were user defined.
- An S-function was created for the Background set in the interval $[x_r, x_{max}]$ and used to assign values to the membership function μ_S. Note that μ_S should contain a membership value for each grey level present in **X**.
- A Z-function was created for the Object set in the interval $[x_{min}, x_j]$ and used to assign values to the membership function μ_Z. Note that μ_Z should contain a membership value for each grey level present in **X**.

$$Z(x_l, x_r, x) = 1 - S(x_l, x_r, x)$$

- The linear index of fuzziness for the Background set was found as follows (Tizhoosh, 2005):

$$\gamma(\text{Background}) = \frac{2}{MN} \sum_{g=0}^{L-1} h(g) \times \min[\mu_S(g), 1 - \mu_S(g)]$$

where the image is MxN pixels with L grey levels and the histogram is h(g).

- The linear index of fuzziness for the Object set was found in the same manner as above.
- α can now be found:

$$\alpha = \frac{\gamma(\text{Background})}{\gamma(\text{Object})}$$

- To compare the IFs of the Background and the Object set when in the fuzzy interval $[x_j, x_r]$ the Object set was multiplied with $\acute{\alpha}$.

4. Each grey level in the fuzzy area was then assigned to either the Background or Object set. This was done by moving from x_j to x_r incrementally and recomputing γ(Background) and γ(Object) with the new grey level.
5. If γ(Background + new grey level) is less than $\alpha.\gamma$(Object + new grey level) then the new grey level was included in the Background set otherwise it was included in the Object set.

6. The threshold point was found by the intersection point of the normalised curves of the indices of fuzziness. The final crisp subset Background was composed of all the grey levels above the intersection point and the crisp subset Object by all the grey levels below the intersection point.

7.2 COLOUR SEGMENTATION

The three techniques used for colour segmentation are given below.

7.2.1 Colour Edge Extraction

This method was taken from Fan et al. (2001) who obtained very good results when used to perform edge detection on images of human faces. It gave very detailed edge detection and performed better than Sobel, Roberts and Prewitt operators run on the same images. To perform the colour-edge extraction, the following method was used:

1. The chosen image was read into MATLAB using the `'imread'` command and was converted from the RGB colour map to the YUV colour map by using the command `'rgb2ycbcr'`.

2. The Edge strength in the horizontal (HOE), vertical (VOE), northeast diagonal (NOE) and northwest diagonal (SOE) of each pixel in the luminance (Y) component was found. The following masks of weighted pixel values were used:

1	2	1
0	0	0
-1	-2	-1

HOE

1	0	-1
2	0	-2
1	0	-1

VOE

2	1	0
1	0	-1
0	-1	-2

NOE

0	1	2
-1	0	1
-2	-1	0

SOE

From these edge strength values the local maximum edge strength of pixel (x,y) MOE(x,y) was found. MOE(x,y) was the maximum of the four edge strengths.

3. The pixels were then classified into edge or non-edge pixels. Given an optimal threshold (T_y) (method for determination given below) Y_{edge} classification function was:

$$Y_{edge}(x,y) = \begin{cases} 1, \text{ edge pixel}, & \text{if } MOE(x,y) \geq T_y \\ 0, \text{ non-edge pixel}, & \text{if } MOE(x,y) < T_y \end{cases}$$

4. Step 2 was repeated for the two chrominance components U and V.

5. For the chrominance component U and the optimal threshold (T_U):

$$\underline{U}_{edge}(x,y) = \begin{cases} 1, \text{ edge pixel,} & \text{if } UOE(x,y) \geq T_U \\ 0, \text{ non-edge pixel,} & \text{if } UOE(x,y) < T_U \end{cases}$$

For the chrominance component V and the optimal threshold (T_v):

$$\underline{V}_{edge}(x,y) = \begin{cases} 1, \text{ edge pixel,} & \text{if } VOE(x,y) \geq T_V \\ 0, \text{ non-edge pixel,} & \text{if } VOE(x,y) < T_V \end{cases}$$

6. The edge results for the three colour components were then integrated together in the following way:

$$\underline{E}(x,y) = \begin{cases} 1, \text{ edge pixel,} & \text{if } (Y_{Edge}(x,y) = 1) \text{ or } (U_{Edge}(x,y) = 1) \text{ or } (V_{Edge}(x,y) = 1) \\ 0, \text{ non-edge pixel,} & \text{otherwise} \end{cases}$$

The optimal thresholds (T_y, T_U, and T_V) were found in the following manner:

1. Let the local maximum edge pixels (MOE, UOE and VOE) have a range of strengths [0, M]. In an input image it was assumed there were f_i pixels whose local maximum edge strength had the value i, $i \varepsilon [0, M]$.

2. The probability for the non-edge pixels $P_n(i)$ were defined as:

$$P_n(i) = \frac{f_i}{\sum_{h=0}^{T} f_h} \qquad 0 \leq i \leq T$$

where $\sum_{h=0}^{T} f_h$ indicates the total number of pixels that have the local maximum edge strength in the range $0 \leq i \leq T$.

3. The probability for edge pixels $P_e(i)$ were defined as:

$$P_e(i) = \frac{f_i}{\sum_{h=T+1}^{M} f_h} \qquad T+1 \leq i \leq M$$

where $\sum_{h=T+1}^{M} f_h$ indicates the total number of pixels that have the local maximum edge strength in the range $T+1 \leq i \leq M$

4. The entropies for these two classes were then represented by:

$$H_n(T) = -\sum_{i=0}^{T} P_n(i) \log P_n(i)$$

$$H_e(T) = -\sum_{i=T+1}^{M} P_e(i) \log P_e(i)$$

5. The optimal threshold T was chosen to satisfy the following criterion function:

$$H(T) = \max_{T=0,1,2,\ldots M} \{H_n(T) + H_e(T)\}$$

Note: If processing time is of concern, the algorithm to find T can be performed recursively (see Fan et al., 2001).

7.2.2 Canny Edge Detection

This Canny edge detection method was successfully used by Ihlow and Seiffert (2003) to segment dyed barley cells from a colour microscopy image. Canny edge detection is a powerful edge detection technique. It uses a filtering mask which finds edges by looking for the local maxima of the gradient of the image (MATLAB, 2002). The gradient of the image *I* is calculated by the derivative of a Gaussian filter with a scale parameter σ that determines the spatial selectivity of the high-pass filter (Ihlow and Seiffert, 2003):

$$\frac{\delta I}{\delta x} \approx I * \left(\frac{-x}{\sigma^2} e^{-\frac{x^2+y^2}{2\sigma^2}} \right) \qquad \frac{\delta I}{\delta y} \approx I * \left(\frac{-y}{\sigma^2} e^{-\frac{x^2+y^2}{2\sigma^2}} \right)$$

This was very similar to the task of segmenting bacteria, thus the following method was used:

1. The chosen image was read into the MATLAB environment using the `'imread'` command. The image was converted from the RGB colour space to the HSV colour space using the `'rgb2hsv'` command.
2. The upper and lower thresholds for the Canny operator as well as a sigma value were chosen.
3. A Canny edge detector was run on the hue component of the image using the `'edge'` command

4. Morphological operations (see below) can be applied to the segmented image by using the `'imdilate'` (for dilation) and `'imopen'` (for opening) commands. The dilation ensured that all of the bacilli were within the boundaries of the segmented image, while the opening removed segmented objects too small to be bacilli.

Morphological Operators

Morphological operators are a broad set of image processing operations that process images based on shapes (MATLAB, 2002). The value of each pixel in the output image is based on a comparison of the corresponding pixel in the input image with its neighbours. By choosing the size and shape of the neighbourhood, a morphological operation is constructed that is sensitive to specific shapes in the input image. This neighbourhood is known as a structuring element. The most basic morphological operations are dilation and erosion.

- **Dilation**: This sets the pixel that is being processed to the maximum value of the pixels included in the structuring element neighbourhood. Dilation adds pixels to the boundaries of objects in an image.
- **Erosion**: This sets the pixel that is being processed to the minimum value of the pixels included in the structuring element neighbourhood. Erosion removes pixels on object boundaries.

Erosion followed by dilation of an image is called opening. Opening is used to remove small objects from an image while preserving the shape and size of larger objects in the image.

7.2.3 Colour Compensation Thresholding

This method was based on the colour compensation technique developed by Castleman (1998). The thresholding and use of the colour compensation in this application were the author's own design. Castleman (1998) intended colour compensation to be used as a technique to separate different fluorophores in fluorescent microscopy, but the use of this technique for image segmentation was not considered. Colour compensation thresholding involves the use of colour compensation techniques followed by crisp thresholding.

1. The chosen image was read into the MATLAB environment using the `'imread'` command.
2. The average amounts of red, green and blue in a typical bacillus in the image were calculated.
3. From the averages, the percentage of each colour present in the bacillus was calculated.
4. The Black level for each colour channel was found by finding the minimum intensity present in each channel in the whole image. The respective Black levels of each colour were then subtracted from the colour of each pixel in the original image to form $I_{modified}$

5. A modified colour spread matrix was formed in the following way:

$$C_{spread} = \begin{bmatrix} \text{Red avg} & 0 & 0 \\ \text{Green avg} & 1 & 0 \\ \text{Blue avg} & 0 & 1 \end{bmatrix}$$

6. The inverse (C_{spread}^{-1}) of the C_{spread} matrix was found by using the `'inv'` command.
7. Colour spread was removed from the image by multiplying C_{spread}^{-1} and $I_{modified}$. The result gave an image (I_{comp}) that was corrected for colour spread and was thus colour compensated.
8. The colour channel in I_{comp}, that showed the bacteria most clearly, was filtered by using a median filter to remove some of the noise that was present. A median filter is very similar to an averaging filter except that it less sensitive to random extreme values (caused by noise) in the image. A median filter was able to remove these extremes without decreasing the image sharpness.
9. A crisp thresholding technique was then performed on the filtered channel.
10. Morphological techniques such as opening were used, where applicable, to rid the final image of small objects.

8 SEGMENTATION RESULTS

This chapter is divided two main sections:

1. **Grey-scale image segmentation results**: This section details the results of applying the crisp and fuzzy thresholding to the images.
2. **Colour image segmentation results**: This section details the results from the colour edge extraction algorithm, the Canny edge detection algorithm and the colour compensation thresholding algorithm when applied to the images.

8.1 THE IMAGES USED

The images used were from two sources:

1. **The smart microscope**: 20 in-focus test images were taken using the smart microscope (See Table 12). The images were all taken using 40x magnification.
2. **A conventional microscope**: 4 images captured for a previous thesis project (Edlauer, 2004) were used.The camera from the smart microscope was attached to a conventional microscope. (see Table 13).

Both sets of images were taken from ZN stained sputum slides. All of the images contained TB bacilli and occasionally other bacilli (e.g. *candida*), fibrin or mucous.

In ZN stained images the TB bacteria should show up red against a blue background. In the images taken from the microscope, the background was not very blue. This could have been caused by the light source of the smart microscope or by the light response of the camera. However the bacteria did show up as red, thus the images were still viable. Because many people with TB are immuno-compromised other bacteria are also present in the sputum smears. However they do not stain red in the manner of the TB bacilli and are often a lot larger (see Figure 17). The images taken from Edlauer (2004) show the red TB bacteria against a blue background. These are classic examples of ZN staining (see Figure 18).

Good image segmentation occurs if only the TB bacilli are segmented from the image.

Table 12 The images from the smart microscope on which the segmentation algorithms were tested.

 Slide Test1	 Slide Test2	 Slide Test3	 Slide Test4	 Slide Test5
 Slide Test6	 Slide Test7	 Slide Test8	 Slide Test9	 Slide Test10
 Slide Test11	 Slide Test12	 Slide Test13	 Slide Test14	 Slide Test15
 Slide Test16	 Slide Test17	 Slide Test18	 Slide Test19	 Slide Test20

Table 13 The images taken on a conventional microscope from Edlauer (2004)

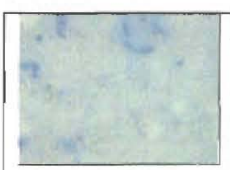 Slide Tech1	 Slide Tech2	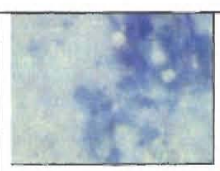 Slide Tech3	 Slide Tech4

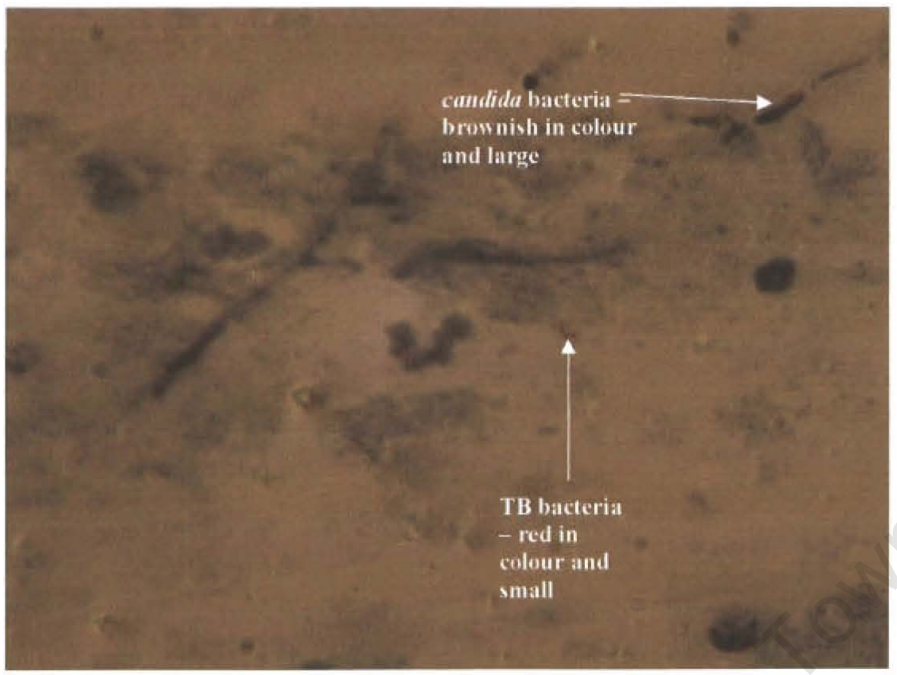

Figure 17 Slide Test16 showing differences between TB and *candida* bacteria

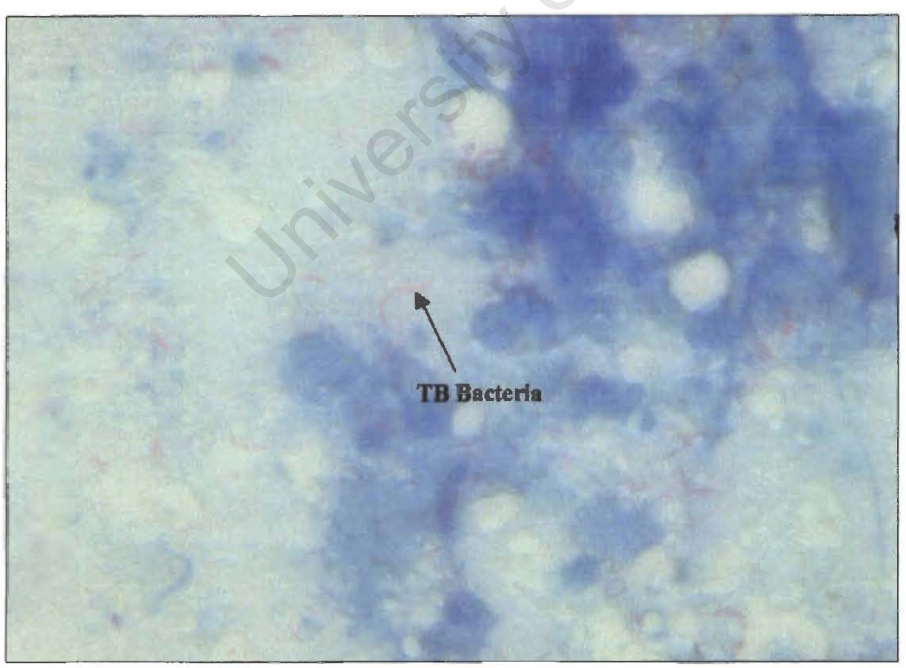

Figure 18 Slide Tech3 showing the red TB bacteria against a blue background (Edlauer, 2004)

8.2 GREY SCALE IMAGE SEGMENTATION

The grey-scale image segmentation results from slides Test1 and Tech3 from the two slide groups are shown. These images are the most typical of the images obtained from each source.

8.2.1 Crisp Thresholding

Slide Test1

Figure 19 shows the results of crisp thresholding (threshold chosen to be 85) on slide Test1. As can be seen in the histogram the grey levels indicating the background and the object are not easily separated. The threshold value of 85 was arrived at through trial and error to see which grey value gave an acceptable segmentation result. The outlined grey-scale image, shows where the segmentation took place. The bacteria were not easily distinguishable in the grey-scale image. The original colour image shows how accurately the segmentation occurred. As can be seen, many objects in the image, which are not bacilli, were segmented. This is because the bacteria in the grey-scale image have the same intensity as many of the other objects in the image. Thus when the bacteria were segmented, so were the other objects.

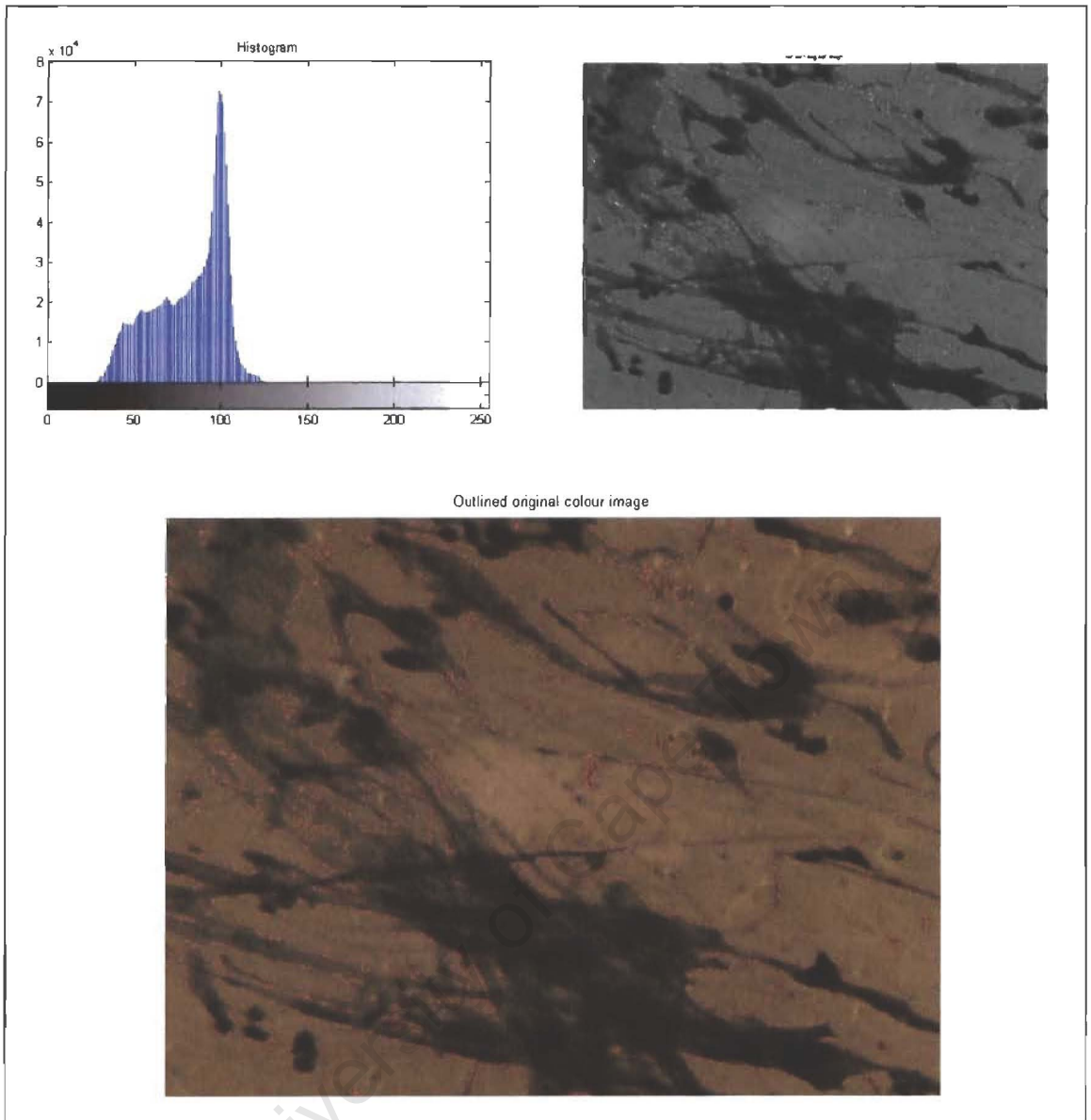

Figure 19 Crisp thresholding of Slide Test1. This shows the grey level histogram, the segmented grey-scale image and the corresponding segmented colour image

Slide Tech3:

Figure 20 shows the results of crisp thresholding (threshold chosen to be 177) on slide Tech3. Again the grey levels indicating the background and the object in the histogram are not easily separated. The threshold value of 177 was arrived at through trial and error to see which grey value gave an acceptable segmentation result. The outlined grey-scale image, shows where the segmentation took place. Again the bacteria were not easily distinguishable in the grey-scale image and the original colour image shows how accurately the segmentation occurred. As can be seen, many objects in the image, which are not bacilli, were segmented. This is because the

bacteria in the grey-scale image have the same intensity as many of the other objects in the image. Thus when the bacteria were segmented, so were the other objects.

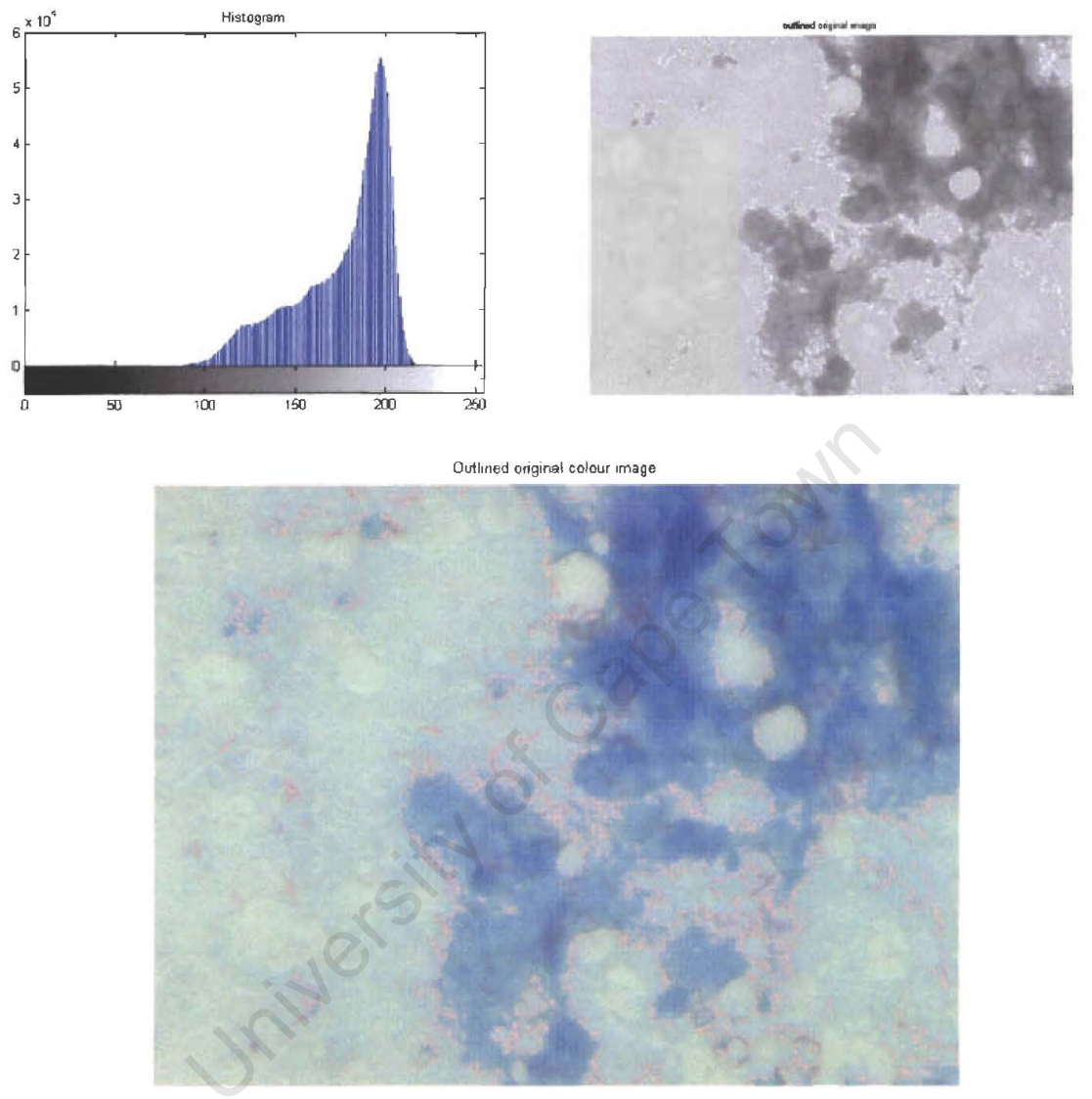

Figure 20 Crisp thresholding of slide Tech3. Showing the grey level histogram, the segmented grey-scale image and the corresponding segmented colour image

As can be seen from the outlined original images of slides Test1 and Tech3, crisp thresholding not only segmented the bacteria but also segmented other aberrations on the slide. It was very tedious and difficult to choose the threshold point, as the histograms make no clear delineation between the background grey levels and the bacteria grey levels. No shape or colour information was taken into account in crisp thresholding.

8.2.2 Fuzzy Thresholding

The following pages show the results of the fuzzy thresholding algorithm applied to the image Test 1 taken by the smart microscope and Tech3 taken from Edlauer (2004).

Slide Test1

Figure 21 shows the results of fuzzy thresholding on slide Test 1. The histogram was equalised to increase the contrast in the image. The Object and Background sets were formed by using Z- and S-functions respectively. The starting fuzzy interval, $[x_j, x_r]$, was chosen through trial and error to be [40, 170]. The threshold value of 88 was found by the intersection of the two fuzzy indices. The third image in Figure 21, the outlined original image, shows how accurately the segmentation occurred. The threshold chosen by the fuzzy thresholding was nearly the same as that for the crisp thresholding and a very similar result was found. As can be seen, in addition to the bacilli many other objects in the image have been segmented. Again, this was for the same reason as that in the crisp thresholding. The bacteria have the same intensity as many objects in the image and therefore cannot be segmented without these objects.

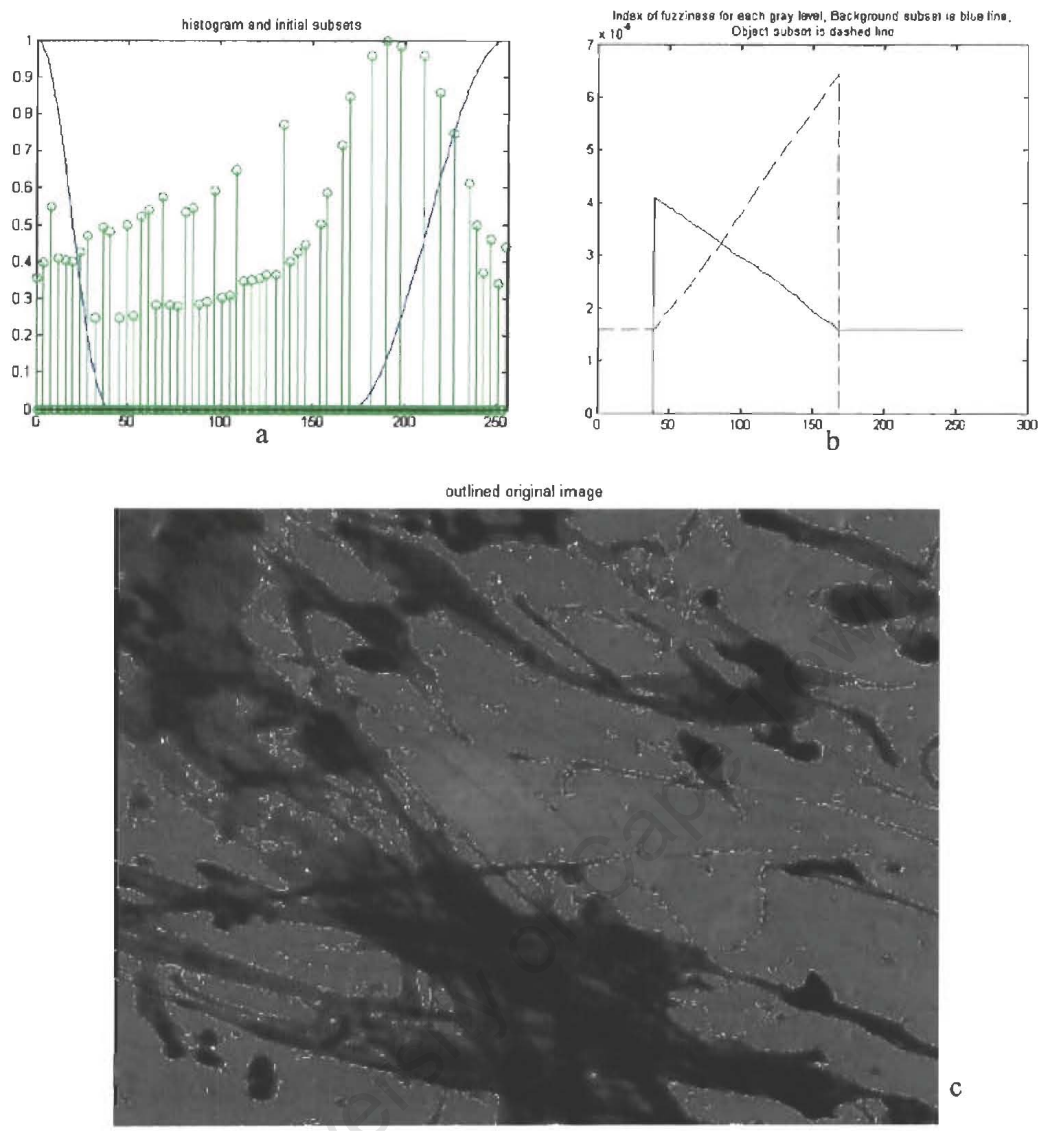

Figure 21 Fuzzy thresholding of slide Test1. a) Equalised histogram showing the initial subsets (Object subset: LHS, Background subset: RHS). b) Indices of fuzziness. c) Original grey-scale image showing outlines where segmentation has occurred.

Slide Tech3:

Figure 22 shows the results of fuzzy thresholding on slide Tech3. The histogram was equalised to increase the contrast in the image. The Object and Background sets were formed by using Z- and S-functions respectively. The starting fuzzy interval, $[x_l, x_r]$ was chosen through trial and error to be [90, 220]. The threshold value of 177 was found by the intersection of the two fuzzy indices. The third image in Figure 22, the outlined original image, shows how accurately the segmentation occurred. As can be seen, a number of objects in the image which are not bacilli were segmented,

and the bacteria were under-detected. In grey-scale images, bacteria have the same intensity as many objects in the image and therefore cannot be segmented without these objects.

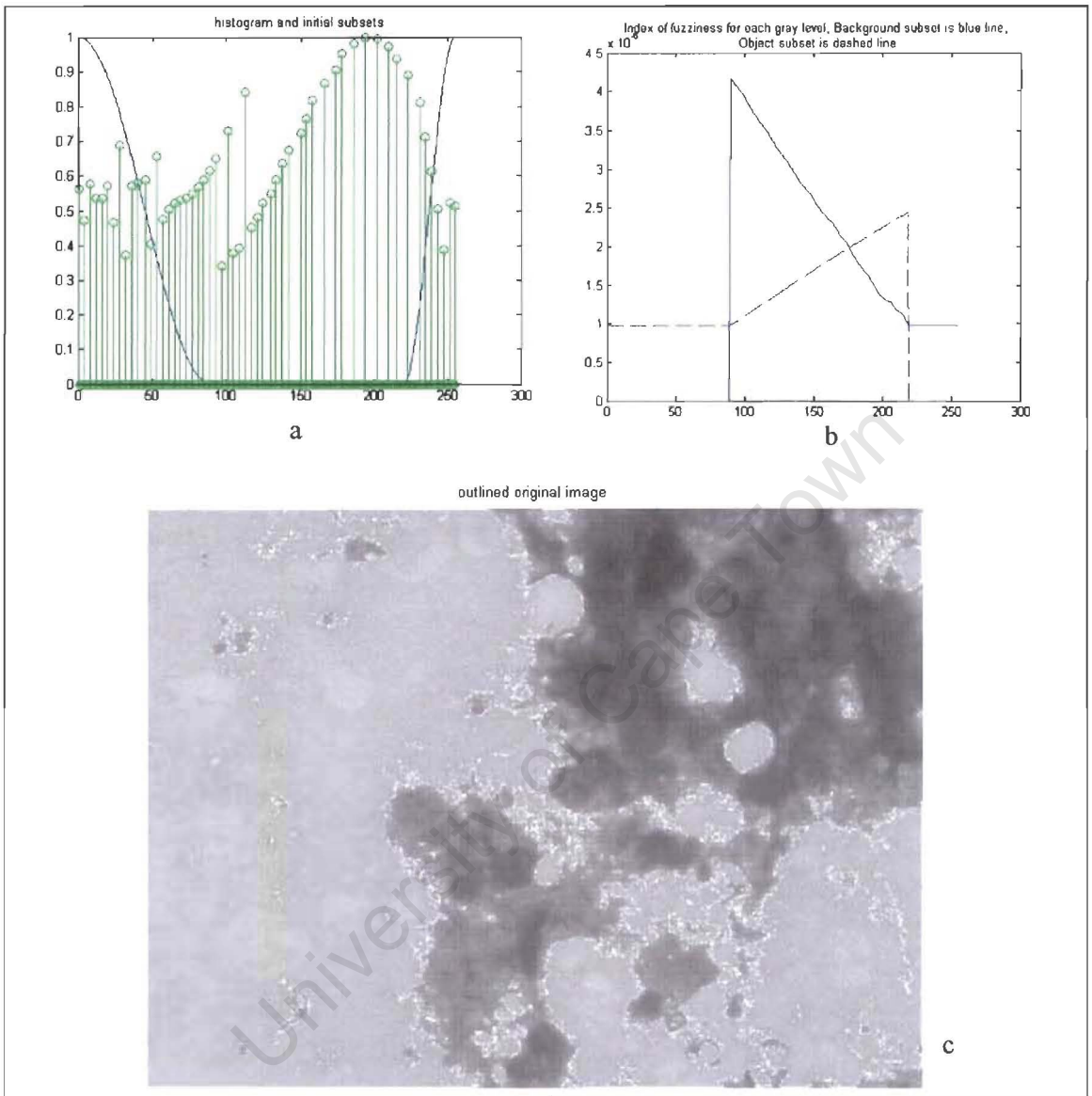

Figure 22 Fuzzy thresholding of slide Tech3. a) Equalised histogram showing the initial subsets (Object subset: LHS, Background subset: RHS). b) Indices of fuzziness. c) Original image showing outlines where segmentation has occurred.

Fuzzy thresholding shows no increase in accuracy of segmentation over the easier to implement crisp thresholding. The starting fuzzy intervals were not consistent for each slide, and badly chosen intervals led to an improperly segmented output image.

8.3 COLOUR IMAGE SEGMENTATION

The colour image segmentation results from slides Test1 and Tech3 from the two slide groups are shown. These images are the most typical of the images obtained from each source.

8.3.1 Colour Edge Extraction

Slide Test1

The threshold intensity values found for each of the channels (Y, U and V) were (see section 7.2.1 for the explanation on how these thresholds were found):

- Ty = 111
- Tu = 114
- Tv = 169

Figure 23 shows the results of colour edge extraction run on slide Test1 obtained by the smart microscope. The binary edge detected image was the sum of the result of the four edge detectors run on each of the channels in the YUV image. The outlined original image was the binary image superimposed on the original slide. The image is over-detected and the shapes of the bacteria are barely discernable.

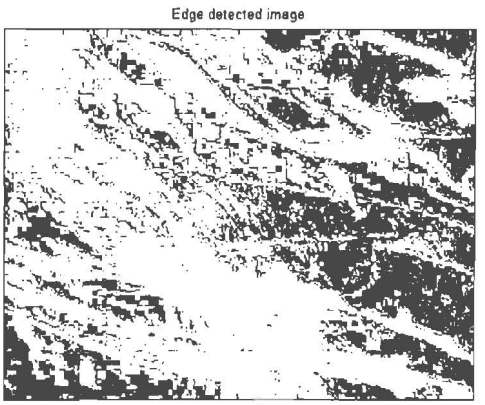

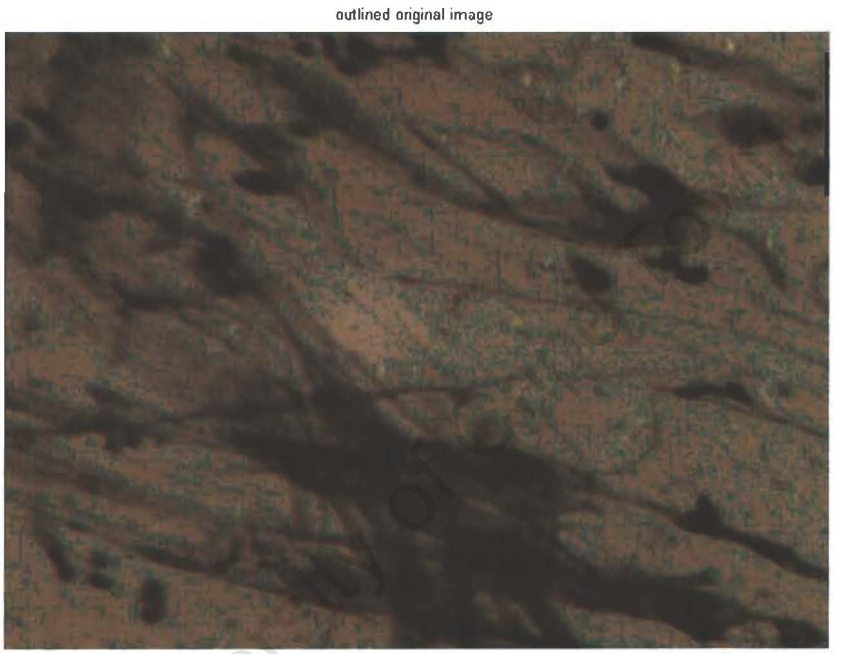

Figure 23 Colour edge extraction of slide Test1. A binary edge detected image and the outlined original image

Slide Tech3

The threshold intensity values found for each of the channels (Y, U and V) were (see section 7.2.1 for the explanation on how these thresholds were found):

- Ty = 668
- Tu = 266
- Tv = 199

Figure 24 shows the results of colour edge extraction run on slide Tech3 obtained from the conventional microscope. The binary edge detected image was the sum of the result of the four edge detectors run on each of the channels in the YUV image. The binary image was nearly

completely black, indicating that virtually no edges were detected in this image. The outlined original image was the binary image superimposed on the original slide. The image was under detected and the bacteria were not detected at all.

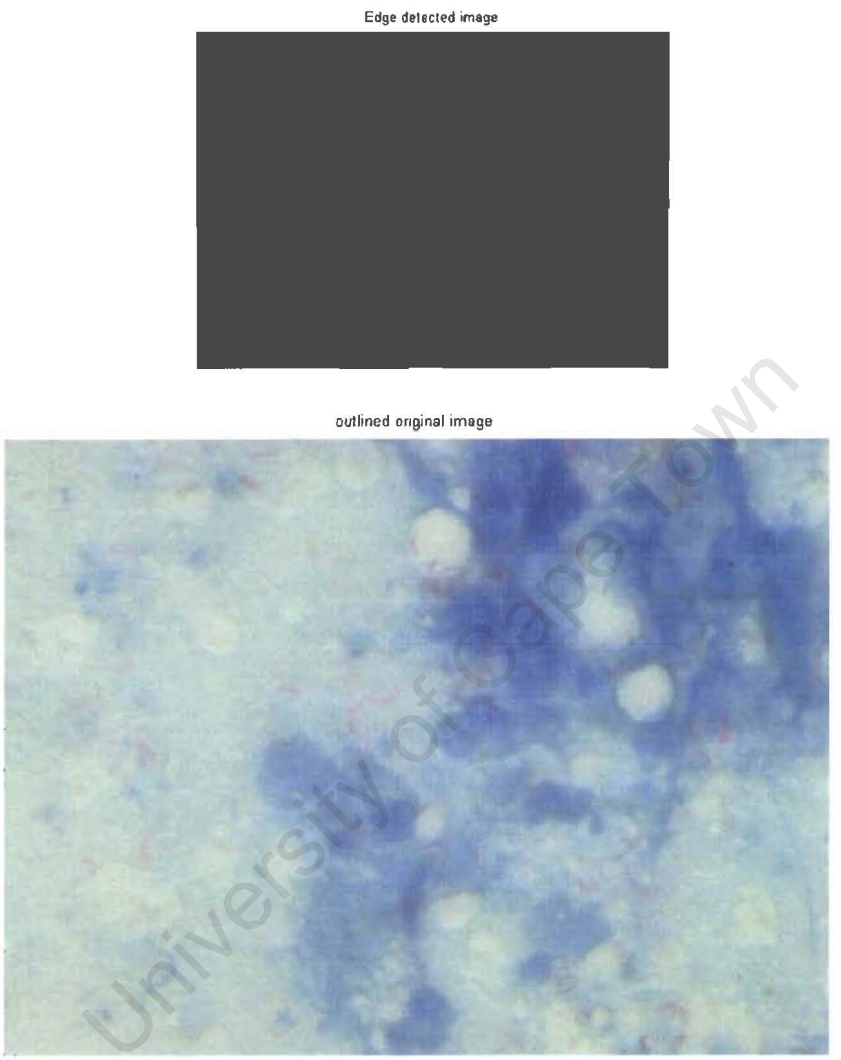

Figure 24 Colour edge extraction of slide Tech3. A binary edge detected image and the outlined original image

The edge detectors in this method were influenced by changes in luminance and chrominance. However from the results seen above, neither the 'Test' slides nor the 'Tech' slides appeared to have enough variations in luminance and chrominance to make this a viable method.

8.3.2 Canny Edge Detection

Slide Test1

The upper and lower thresholds for the Canny edge detector were chosen to be [0; 0.05], while the sigma value chosen was 12. Figure 25 shows the results of the Canny edge detector run on Slide Test1 obtained by the smart microscope. The binary edge detected image was the result of the Canny edge detector run on the hue channel of the image. The binary image was then superimposed onto the hue channel, and after being opened and dilated (a disk of 5 pixels was used to dilate the image, while a disk of 8 pixels was used to open the image) it was then superimposed onto the original slide. The TB bacteria hardly show up in the hue channel. This was an unexpected result as in the original image they appear red in colour, so it was expected that they would show up red in the hue channel. The Canny edge detector struggled to recognise the bacteria in the image. It also detected some of the background to be bacteria. With a low value for sigma (such as 1 or 5) the bacteria were not recognised at all, thus a 'rigorous' sigma of 12 was used.

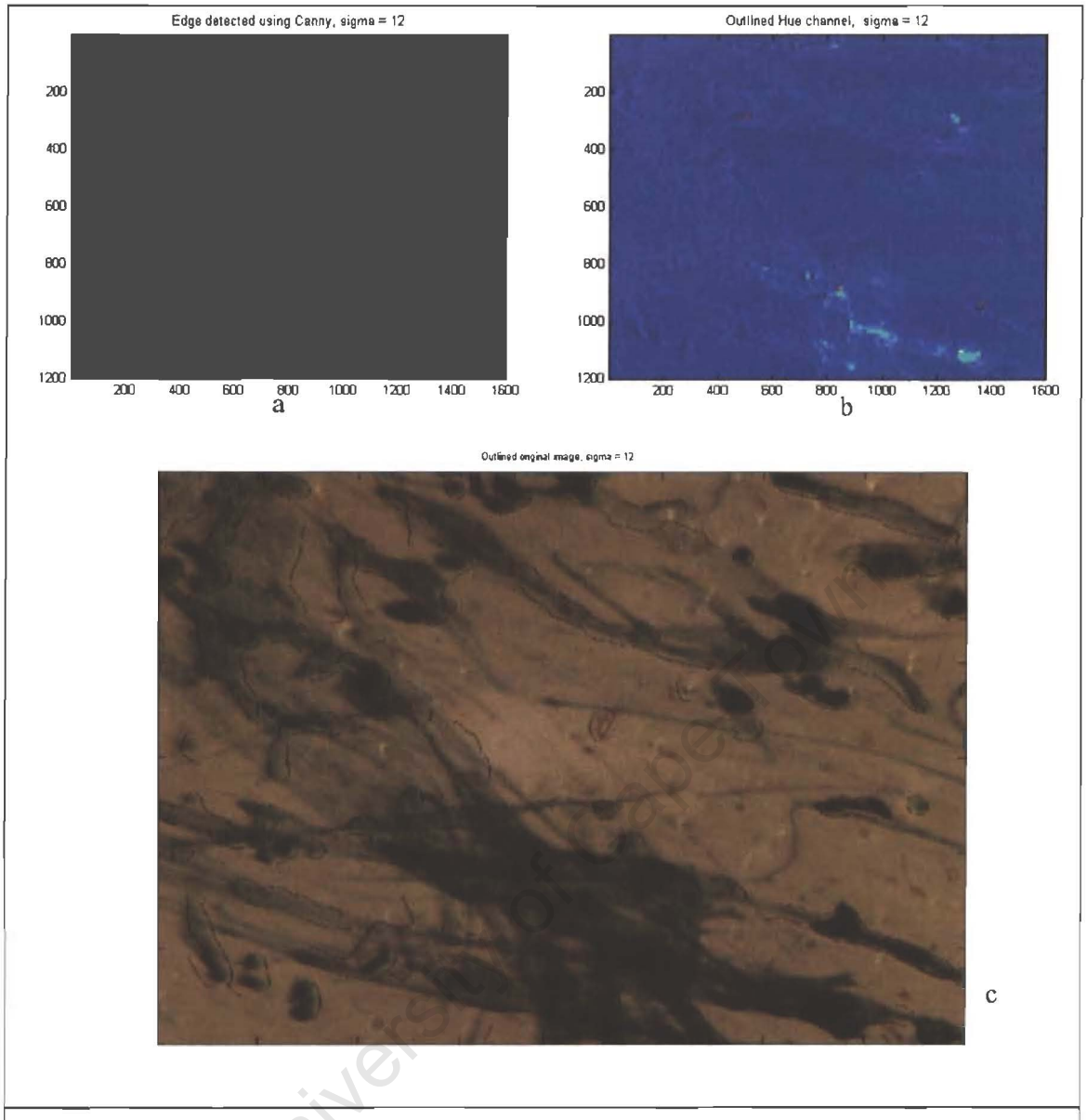

Figure 25 Canny edge detection of slide Test1. a) Binary image of edge detected slide. b) The binary image overlaid on the hue channel. c) The binary image (opened and dilated) overlaid on the original

Slide Tech3

The upper and lower thresholds for the Canny edge detector were chosen to be [0.10; 0.30], while the sigma value chosen was 1. Figure 26 shows the results of the Canny edge detector run on slide Tech3, obtained from the conventional microscope. The binary edge detected image was the result of the Canny edge detector run on the hue channel of the image. As can be seen in Figure 26 the hue channel clearly showed a number of the bacteria. The binary image was then superimposed onto the hue channel, and then onto the original slide. The Canny edge detector did not recognise all of the bacteria in the image and some of the background was also detected as bacteria.

Figure 27 shows the results of opening and dilating the image in Figure 26 using morphological structuring elements. A disk of 5 pixels was used to dilate the image, while a disk of 8 pixels was used to open the image (which rids the image of any small unwanted segmented areas).

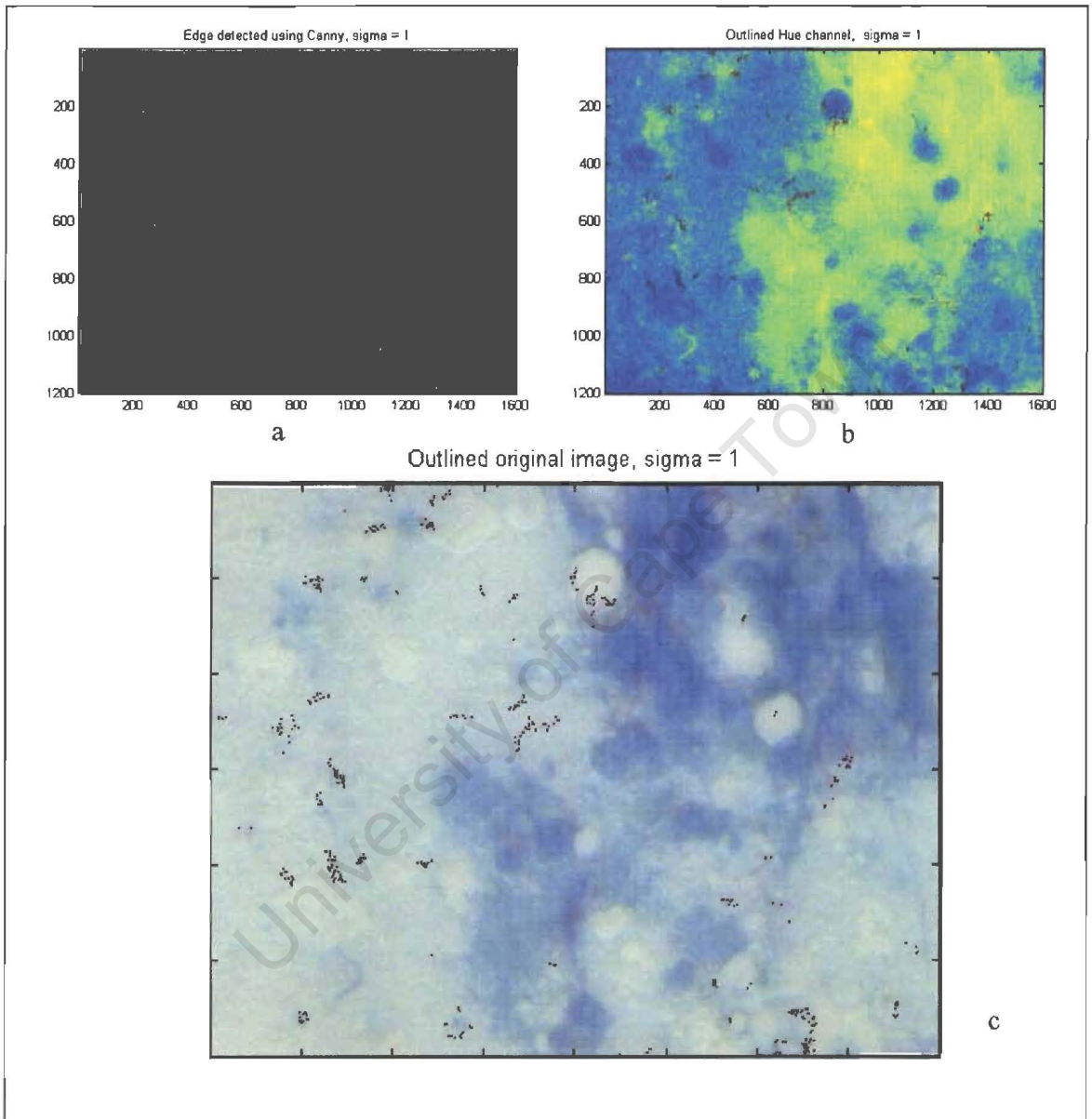

Figure 26 Canny edge detection of slide Tech3. a) Binary image of edge detected slide. b) The binary image overlaid on the hue channel. c) The binary image overlaid on the original image.

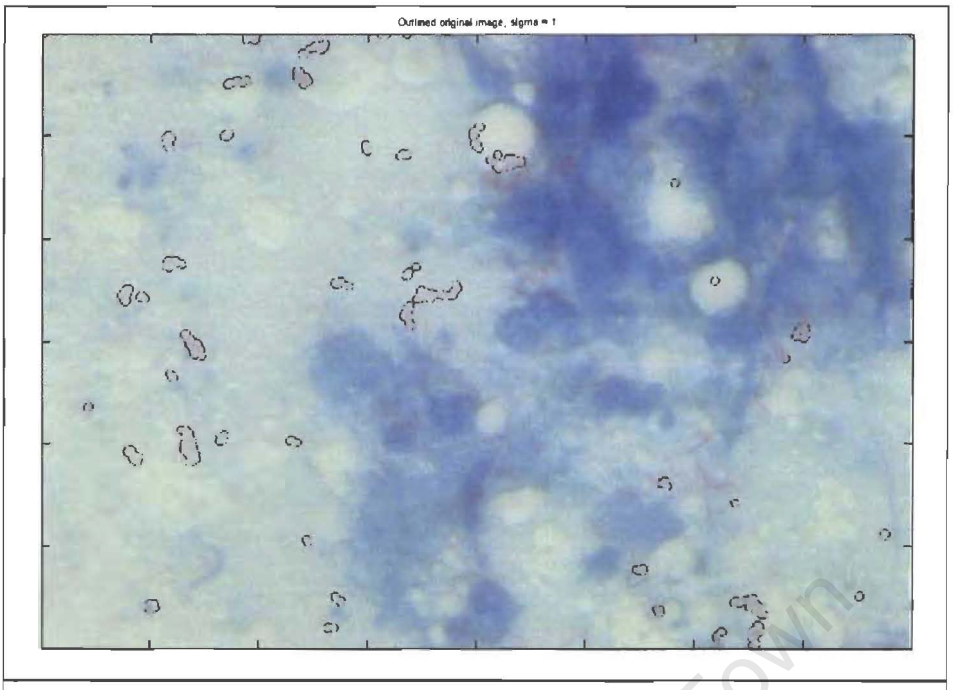

Figure 27 Canny edge detection of slide Tech3. The segmented image of Figure 26 opened and dilated using morphological operators.

8.3.3 Colour Compensation Thresholding

Slide Tech3

Figure 28 shows the colour bands present in the slide Tech3. The top row shows how the red, green and blue colour bands looked before any processing had taken place. The bottom row shows how the colour bands looked after they had been colour compensated. Notice how visible the bacteria are in the corrected green band image. The colour compensation matrix used was (see section 7.2.3 for an explanation on how to obtain and use this matrix):

$$C_{spread} = \begin{bmatrix} 0.3386 & 0 & 0 \\ 0.3276 & 1 & 0 \\ 0.3338 & 0 & 1 \end{bmatrix}$$

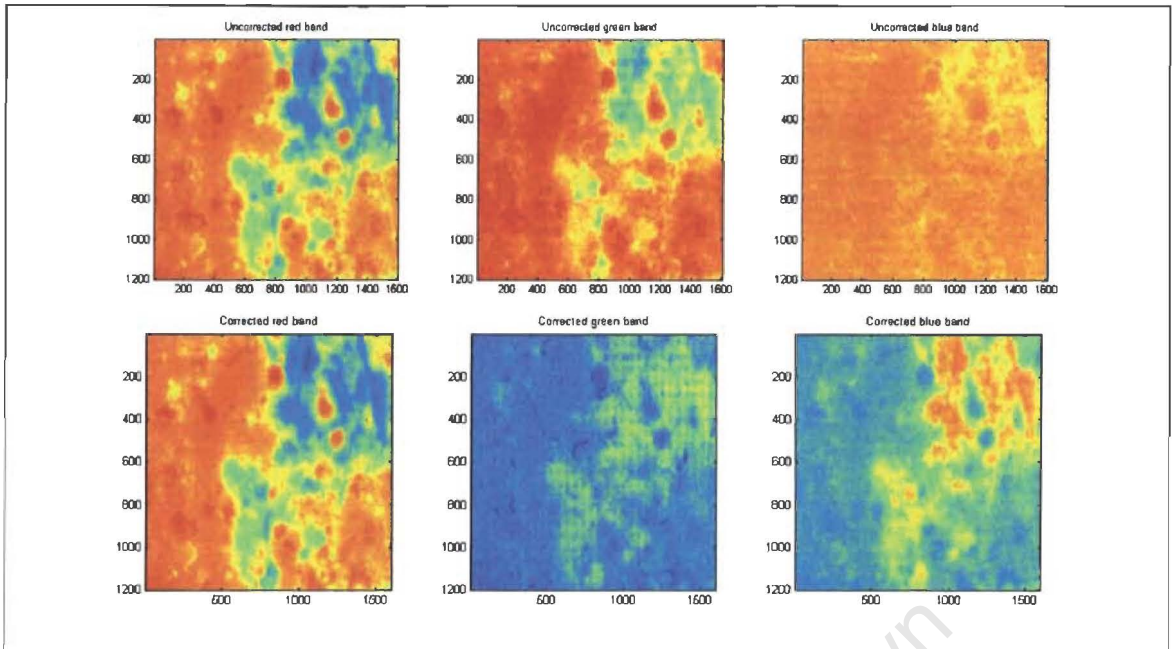

Figure 28 Slide Tech3. The uncorrected colour bands with their respective corrected colour bands (colour spread taken into account). Colour bands are displayed using MATLAB's default colour map.

Figure 29 shows the results of a 5x5 median filter applied to the corrected green colour band to reduce the noise present in the image. This filter was too small to alter the appearance of the bacilli. The image was then thresholded using a crisp thresholding algorithm. The threshold value was chosen to be 12 after inspection of the colour-bar of the median filtered image. The results of this process were then superimposed over the original image. The bacteria were clearly segmented in this image, as shown below. This was a good segmentation result.

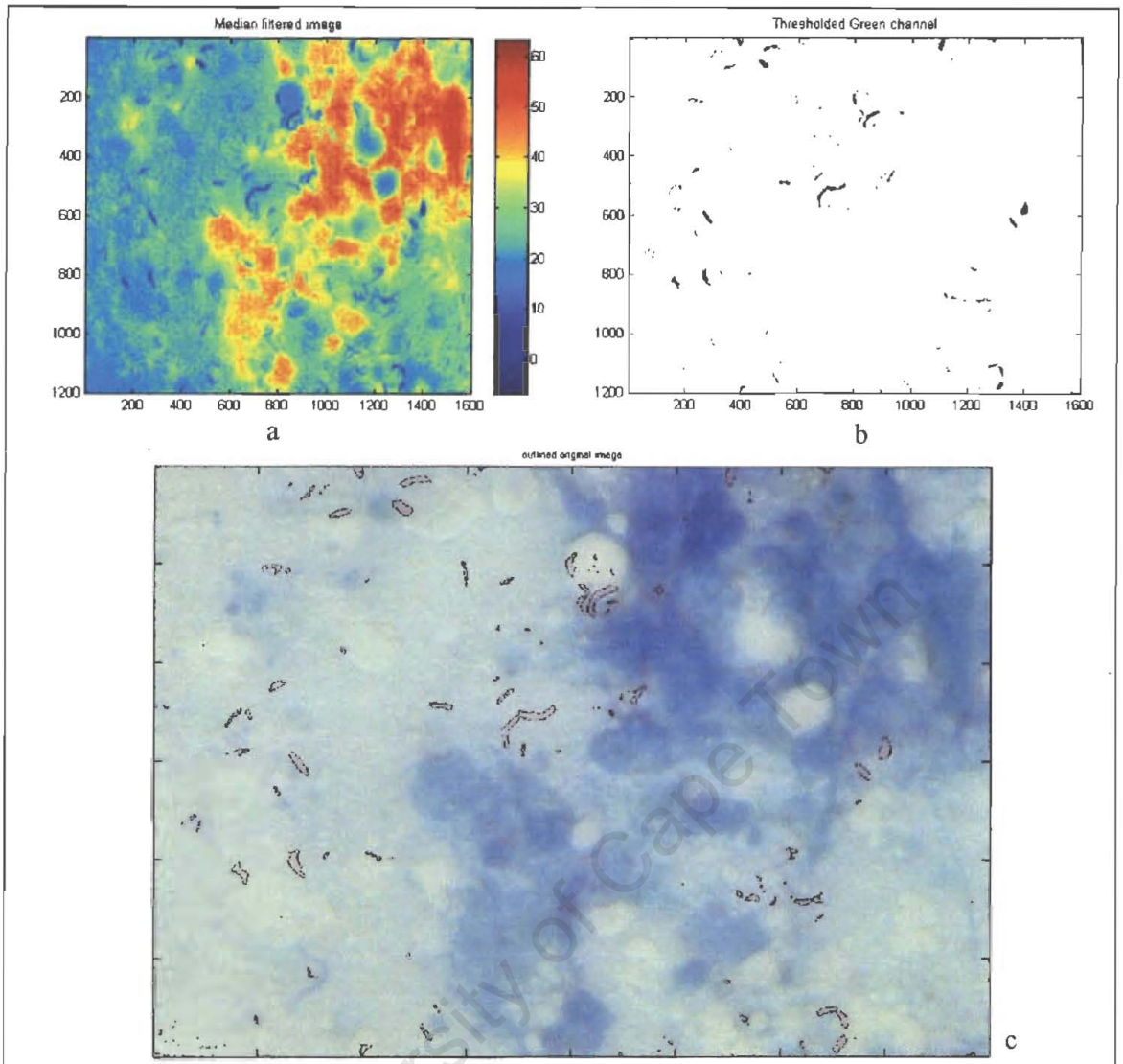

Figure 29 Slide Tech3. a) The corrected green colour band with a median filter applied. b) Crisp Threshold applied to the median filtered image. c) Thresholded image superimposed over original slide image.

Slide Test1

Figure 30 shows the colour bands present in the slide Test1 taken by the smart microscope. The top row shows how the red, green and blue colour bands looked before any processing had taken place. The bottom row shows how the colour bands looked after they had been colour compensated. Notice how visible the bacteria are in the corrected green band image. The colour compensation matrix used was (see section 7.2.3 for an explanation on how to obtain and use this matrix):

$$C_{spread} = \begin{bmatrix} 0.4598 & 0 & 0 \\ 0.3059 & 1 & 0 \\ 0.2343 & 0 & 1 \end{bmatrix}$$

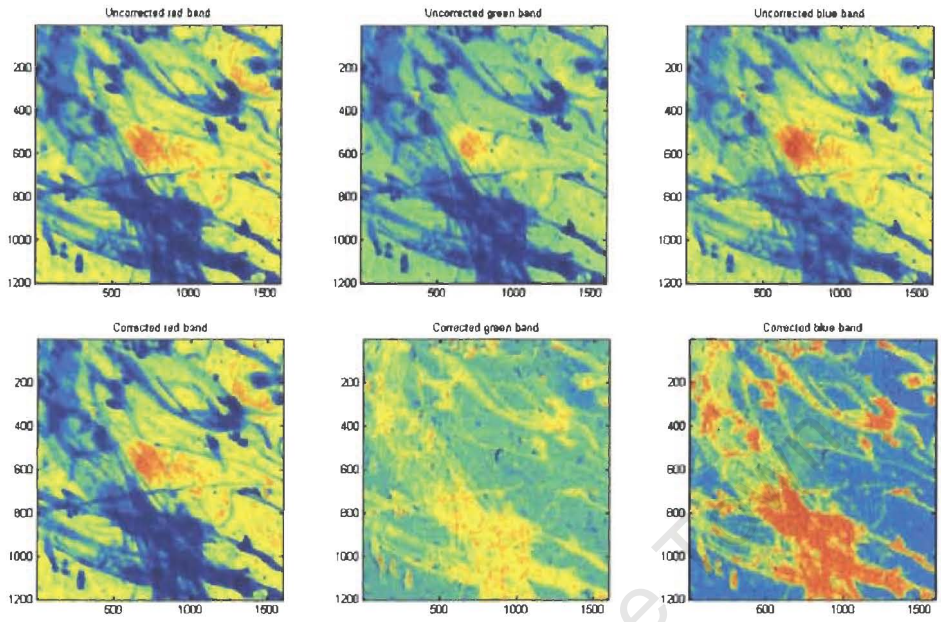

Figure 30 Slide Test1. The uncorrected colour bands with their respective corrected colour bands (colour spread taken into account).

In Figure 31 a 5x5 median filter was applied to the corrected green colour band. This was then thresholded using a crisp thresholding algorithm. The threshold value was chosen to be -3 after inspection of the colour-bar of the median filtered image (not shown in Figure 31). The results of this process were then superimposed over the original image. The bacteria were clearly segmented in this image which was another good segmentation result.

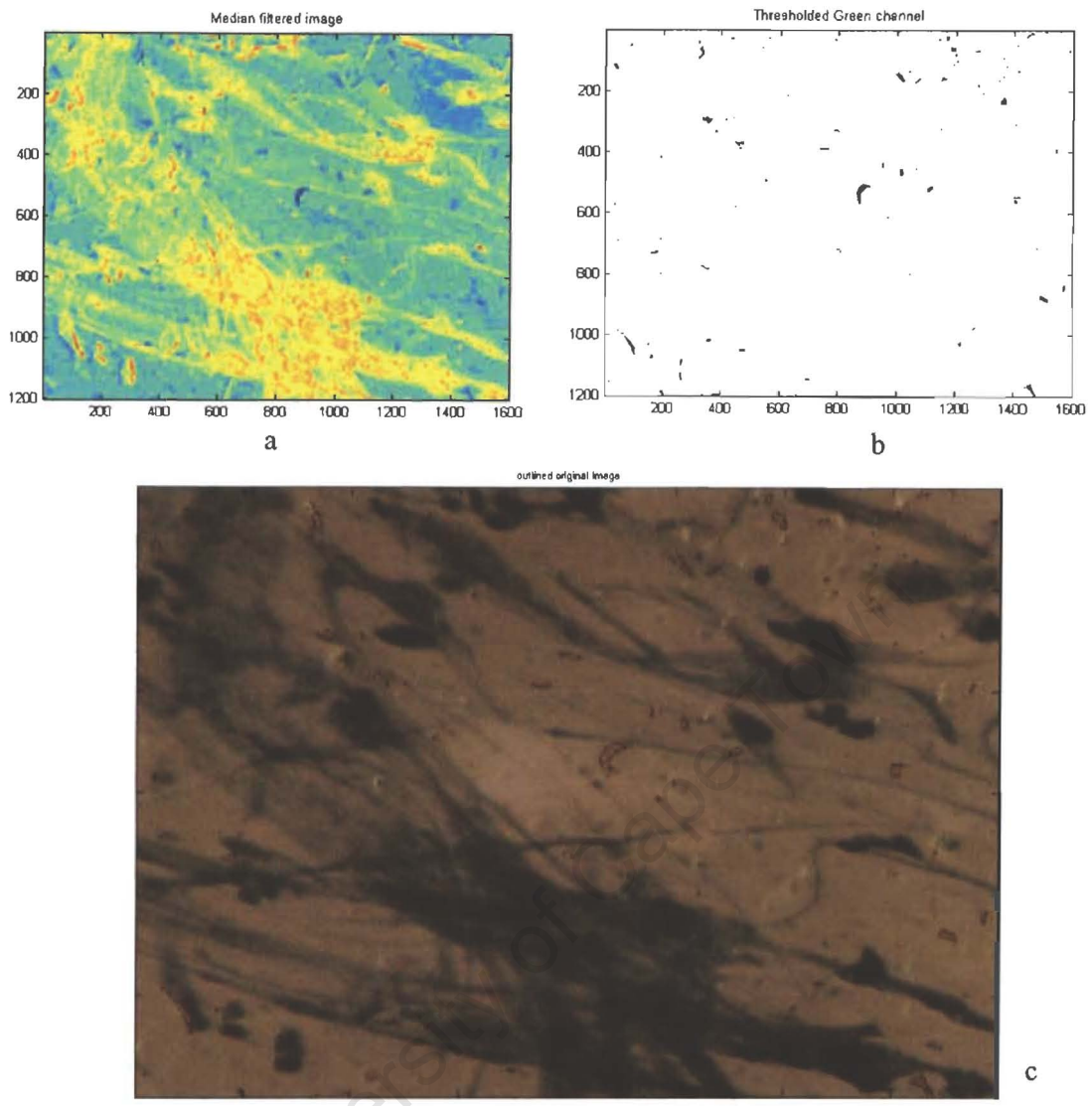

Figure 31 Slide Test1. a) The corrected green colour band with a median filter applied. b) Crisp threshold applied to the median filtered image. c) Thresholded image superimposed over original slide image.

Slide Test2

This is another example from the smart microscope to show how well this method works. A threshold of -3 was used with the following matrix:

$$C_{spread} = \begin{bmatrix} 0.4383 & 0 & 0 \\ 0.3086 & 1 & 0 \\ 0.2530 & 0 & 1 \end{bmatrix}$$

Figure 32 shows the segmented areas in slide Test 2. Again the bacteria were well segmented in the image.

Figure 32 Slide Test2. The original image showing the outlines of the segmented areas.

Using C_{spread} (Average)

As a large set of images containing the TB bacilli were taken using the smart microscope, a C_{spread} matrix containing the average colour values of a TB bacilli was created. This matrix was then used in place of the specialized C_{spread} matrix for each image taken by the smart microscope.

This is calculated in Appendix 12.2 by finding the Cspread matrix for all the slides and then taking the average. C_{spread} (Average) was found to be:

$$C_{spread}\,(\text{Average}) = \begin{bmatrix} 0.44901 & 0 & 0 \\ 0.31450 & 1 & 0 \\ 0.23992 & 0 & 1 \end{bmatrix}$$

In Table 14 the differences between using the image specific matrix for C_{spread} and using the calculated average matrix (C_{spread} (Average)) are shown. The thresholds were found automatically (no user intervention required) by taking a histogram of the median filtered green channel, finding the lowest intensity and then adding 10 units to it, to allow for slight colour variations in the bacteria (the value 10 was chosen by examination of the images). The specific and average results were very similar to each other, with both matrices segmenting the bacteria from the images. Occasionally, when the background contained a lot of red, the image was over-

segmented (e.g. slide Test19), but this was rare. Overall the method of colour compensated thresholding gave very good results.

Table 14 The difference in segmentation results between segmenting the image using the image specific matrix or using the average matrix. Tested using three slides from the smart microscope.

Slide Name	Segmented image using the specific matrix	Segmented image using the average matrix
Test1	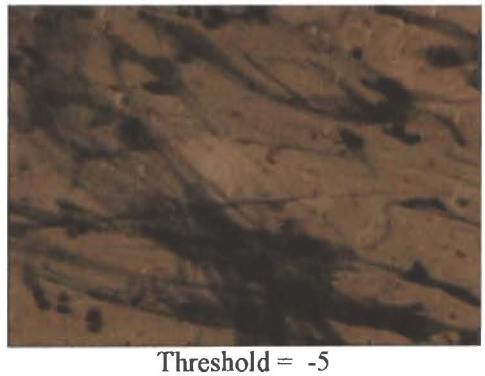 Threshold = -5	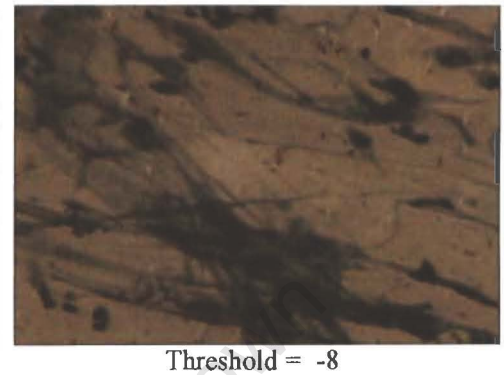 Threshold = -8
Test2	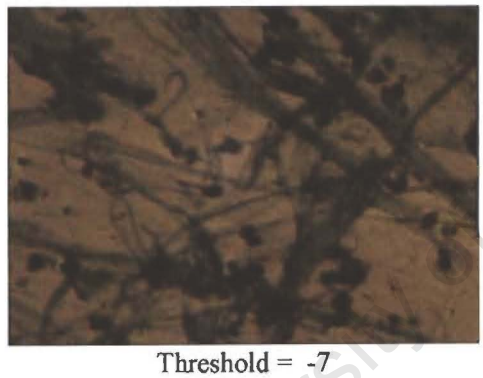 Threshold = -7	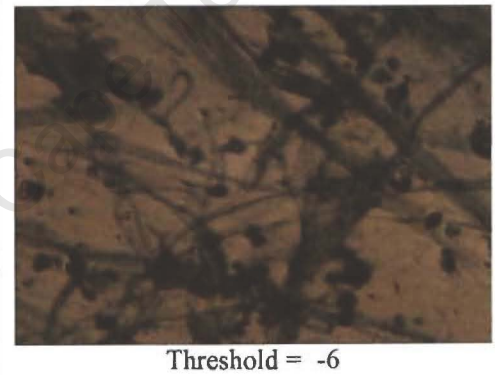 Threshold = -6
Test19	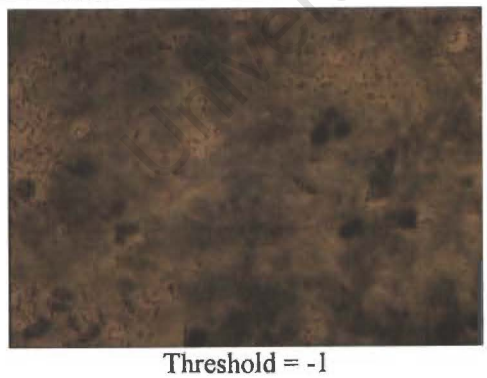 Threshold = -1	 Threshold = 2

Colour Compensation Thresholding Applied to Out-of-focus Images

As the focus of this thesis was autofocusing as well as image segmentation, it was interesting to see whether successful segmentation could occur on images that were slightly out-of-focus. Images from the autofocusing slide series were used; namely slide series 11 to 20 (see Table 4). The colour compensation thresholding algorithm was applied to the focused image and an image 4μm out of focus (as this was the maximum error in the autofocusing algorithm). The absolute value of the difference in the two segmentation results was then found. See Table 15 and Table 16 for some of the results.

Table 15 Showing the colour compensation thresholding algorithm applied to in-focus and out-of-focus images from slide series 13. The difference in the segmentation results is also shown.

Slide series	Segmentation result	Difference in the segmentation results
13 – in-focus	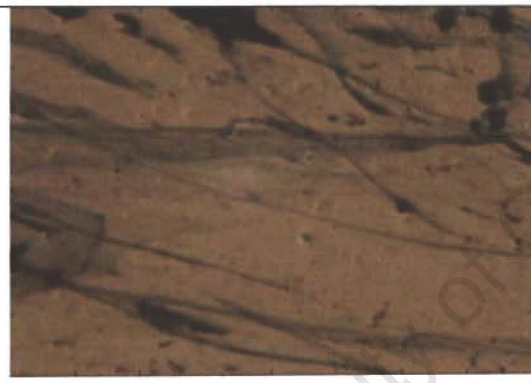	
13 – out-of-focus		

Table 16 Showing the colour compensation thresholding algorithm applied to in-focus and out-of-focus images from slide series 15 and 16. The difference in the segmentation results is also shown.

15 – in-focus		
15 – out-of-focus	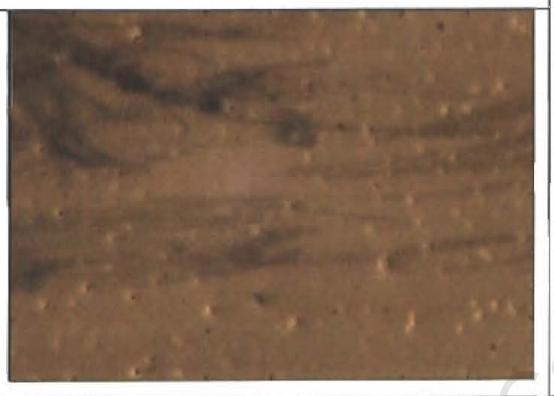	
16 – in-focus		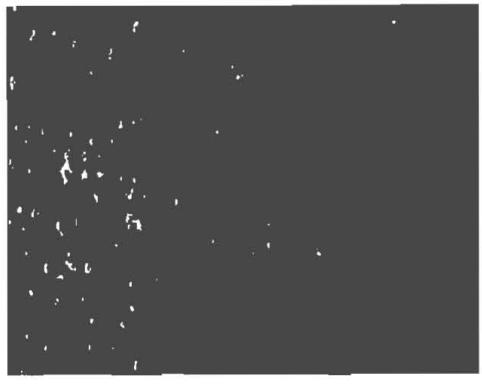
16 – out-of-focus	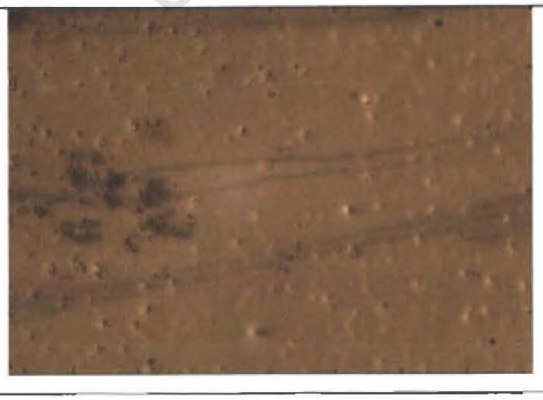	

8.4 SEGMENTATION DISCUSSION

The images taken by the smart microscope were not ideal. They had a very brown background which could be due to the either the camera settings or the light source. The reason for this brown background should be investigated and remedied as it could affect the segmentation results. When Edlauer (2004) took the conventional microscope images the only difference between this and the current smart microscope was the light source: the same camera was used (LU200) and the same objective lens was used (40x magnification with a NA of 0.65). The colour response of the camera could also have contributed to the background colour in the images. As can be seen in Figure 33 the current camera (LU200) has a higher sensitivity to red light than to any other colour. The camera that is now being investigated for use in the smart microscope is the Lumenera LU130. As seen in Figure 33 this camera has a more balanced sensitivity to all colours.

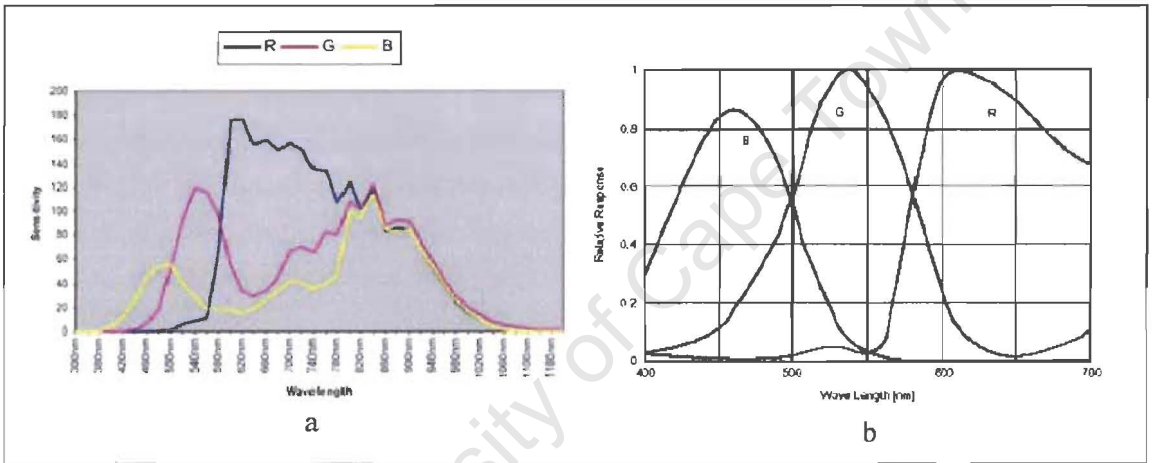

Figure 33 The colour response curves of a) the LU200 and b) the LU130 (Lumenera documentation)

The images taken by the conventional microscope, from Edlauer (2004), were ideal examples of ZN stained sputum smears. The bacteria show up red against a blue background. The segmentation algorithms were applied to both these images and those from the smart microscope. Assessment of the segmentation algorithms should consider the performance of the algorithms on both sets of images.

8.4.1 Grey-Scale Segmentation

There was no great difference in the results from the crisp or the fuzzy thresholding algorithms. In the crisp thresholding results the bacteria could not be segmented from other objects in the image. As the histograms from the image do not have obvious valleys separating the object and background classes, a threshold value was hard to decide upon and a trial-and-error approach was used. This was obviously not an ideal technique for what should be an automated process.

Fuzzy thresholding was then attempted to automate the selection of a threshold value. However in this case, new object and background sets had to be formed in order to find the threshold point. No information about how to choose the sets was given by Tobias and Seara (2002) and thus a trial-and-error approach was again used to choose the initial subsets.

Neither of the thresholding algorithms gave good results. Both required too much user interaction and the final segmentation segmented both the bacteria and other objects from the image. These methods took neither the shape nor the colour of the bacteria into consideration.

8.4.2 Colour Segmentation

Three different methods were applied using colour images. The first method, colour edge extraction, over-detected the images from the smart microscope and barely detected anything in images from the conventional microscope. Colour edge extraction is meant to identify the colour edges in YUV colour space. In other words, differences in the luminance (Y) and in the chrominance (U and V) should be detected. However:

- Images from the smart microscope had a slight increase in luminance in the centre of the image, and this was heavily detected using this method. Small changes in colour, such as between the bacteria and the background were not well detected.
- Images from the conventional microscope had greater changes in colour between the bacteria and the background than images from the smart microscope. However, these were not detected at all. The images from the conventional microscope were quite subtle in their changes in luminance and chrominance and none of these changes were picked up using the colour edge extraction method.

This method was not suitable for the detection of TB bacteria in sputum slides stained with ZN.

Canny edge detection was a method favoured by a number of authors (Veropoulos et al., 1998; Forero et al., 2004) for use in the segmentation of TB bacilli from images of auramine-stained sputum slides. The Canny operator applied to the Hue channel in HSV colour space worked, however it did not differentiate between the bacilli and other objects in the image. Objects which were not bacteria were segmented. This method gave good results on both the images from the smart microscope and from the conventional microscope.

The final colour image segmentation method investigated was colour compensation thresholding. This gave excellent results for both images from the smart microscope and from the conventional microscope, indicating that the brown background colour of images from the smart microscope might not have had a detrimental effect on segmentation. The use of the averaged colour

compensation matrix refined the algorithm to ensure that specifically TB was identified in images taken by the smart microscope.

Both the Canny edge detector and the colour compensation thresholding method gave good results. However the Canny edge detector also tended to segment non-bacteria items in the images. The colour compensation thresholding method generally segmented only the bacteria. This is advantageous because the results from the segmentation stage could potentially be fed directly to a bacillus counting module without the need for classification. Bacillus counting would require the identification and counting of individual segmented objects, with the aid of a method such as the extraction of connected components (Gonzalez and Woods, 1992). Further testing of the specificity of the method should be done in future before direct counting of segmented objects is explored. Automatic thresholding was used in colour compensation thresholding, thus requiring no user interaction. The automatic threshold was acquired by taking the histogram of the image and assigning 10 units to the lowest value.

When the colour compensation thresholding technique was applied to out-of-focus images the images were slightly over-segmented. The bacteria were detected but some of the background and other objects were also detected. Thus it is important that the segmentation algorithm is applied to images that are in-focus.

8.5 Segmentation Conclusion

A number of different methods of image segmentation were applied. The grey-scale methods yielded poor results as they took neither shape nor colour into account. Three different colour image segmentation methods were used. Both the Canny edge detection and the colour compensation thresholding were suitable for use on sputum smear images that contain TB bacilli. However the colour compensation thresholding method gave slightly better and more specific results than the Canny operator as only bacilli were segmented. An average matrix for use in the colour compensation thresholding method was developed. This matrix allowed the method to specifically detect the TB in images taken from the smart microscope, as it took into account the colour that the TB bacilli appeared in these images. If the light source or camera is changed, the colour of the TB bacilli in the image will also change thus the average matrix must be recalculated (see appendix 12.2). Although the bacteria can be detected in a slightly out-of-focus image, the more in-focus the image, the better the segmentation.

9 GENERAL CONCLUSIONS AND RECOMMENDATIONS

9.1 CONCLUSIONS

An autofocusing algorithm has been developed and tested for the smart microscope. The algorithm worked satisfactorily for all the slide series on which it was tested, but it runs more slowly than autofocusing algorithms reported in the literature. The algorithm uses the Energy of the Image Laplacian focus measure and does not use windowing. An autofocusing algorithm for ZN stained sputum slides has, to the author's knowledge, never been reported before.

A number of different methods of image segmentation were applied to both grey-scale and colour images. The grey-scale methods yielded poor results as they took neither shape nor colour into account. Three different colour image segmentation methods were used. Both the Canny edge detection and the colour compensation thresholding were suitable for use on sputum smear images that contain TB bacilli. However the colour compensation thresholding method gave slightly better and more specific results than the Canny operator as it segmented bacilli only. The colour compensation thresholding method, designed by the author, is a new segmentation method based on the colour compensation technique proposed by Castleman (1993). An average matrix for use in the colour compensation thresholding method was developed. This matrix allowed the method to specifically detect the TB in images taken from the smart microscope, as it took into account the colour the TB bacilli appeared in these images. If the light source or camera is changed, the colour of the TB bacilli in the image will change, thus the average matrix must be recalculated (see appendix 12.2). Although the bacteria can be detected in a slightly out-of-focus image, the more in-focus the image, the better the segmentation. Colour compensation thresholding holds promise as a method of segmentation that is specific to TB bacilli, and therefore could remove the need for classification algorithms that discriminate between bacilli and undesirable segmented objects.

The success of segmentation depends on the success of autofocusing. Ensuring an optimal position of focus will mean that the segmentation has the best chance of detecting all the bacteria in the image.

9.2 RECOMMENDATIONS

The following recommendations are made for future work on the smart microscope:

- Investigate the cause of the brownish background in the images from the smart microscope. It could be due to the light source or to the camera model. When the images are more similar to those from a conventional microscope, a new average matrix for the colour compensation method will have to be formed. This is because the colour of the TB bacilli will have changed slightly, and the matrix needs to be specific to whichever colour the TB bacilli appear in an image.
- Determine the sensitivity and specificity of the colour compensation thresholding segmentation algorithm, using bacillus detection by an experienced TB technologist as the gold standard. This will indicate whether all humanly detectable bacilli are being segmented, whether non-bacillus objects are being segmented and whether further classification of the segmented objects is required.
- Rework the code given here from MATLAB code to C++. This will allow faster running time. It will also allow the autofocusing algorithm to be tested whilst connected to the microscope.
- Investigate the staining standards of the sputum slides. The slides must be consistently well prepared. When a slide is badly prepared, mucous may be present on the slide. This stains the same red as the TB bacilli, eliminating any chance of accurate segmentation. A standard ZN staining routine should be investigated, as the intensity of the stain depends on the technician preparing the slide. With a standard staining routine, standard intensities for the bacilli and the background may be possible.
- Implement the 'anti-backlash' setting on the actuators, to ensure that the position of focus always comes from the same direction. It was not necessary to implement this while taking the slide series (as this was done manually, and the position was always approached from the same direction), however it will be vital once the autofocusing algorithm directly controls the position of the smart microscope.

10 REFERENCES

1. Basheer I, Hajmeer M, 'Artificial neural networks: fundamentals, computing, design and application', *Journal of Microbiological Methods*, 43, 2000, pp 3-31
2. Boddeke F, Van Vliet L, Young I, 'Calibration of the automated z-axis of a microscope using focus functions', *Journal of Microscopy*, 1997, 186, pp 270-274
3. Brink A. D, 'Minimum spatial entropy threshold selection', *IEE Proceedings on Visual Image Signal Processing*, Vol. 142, No. 3, 1995, pp 128-132
4. Castleman K. R, 'Color Compensation for digitized FISH images', *Bioimaging*, 1, 1993, pp 159-165
5. Castleman K. R, 'Digital image color compensation with unequal integration periods', *Bioimaging*, 2, 1994, pp 160-162
6. Castleman K. R, 'Concepts in Imaging and Microscopy: Color Image Processing for Microscopy', *Biol. Bull.*, 194, 1998, pp 100-107
7. Cheng H. D, Jiang X. H, Sun Y, Wang J, 'Color image segmentation: advances and prospects', *Pattern Recognition*, 34, 2001, pp 2259-2281
8. Della Mea V, Viel F, Beltrami C, 'A pixel-based autofocusing technique for digital histologic and cytologic slides', *Computerized Medical Imaging and Graphics*, 2005, 29, pp 333-341
9. Edlauer M. 'Automatic Diagnoses of *Mycobacterium Tuberculosis* in Microscope Images of Sputum Samples', Thesis for BSc(Eng) University of Cape Town, 2004
10. Erikson M, 'Two preprocessing techniques based on grey level and geometric thickness to improve segmentation results', *Pattern Recognition Letters*, 27, 2006, pp 160-166
11. Fan J, Yau D. K. Y, Elmagarmid A. K, Aref W. G, 'Automatic Image Segmentation by Integrating Color-Edge Extraction and Seeded Region Growing', *IEEE Transactions on Image Processing*, Vol. 10, No. 10, 2001, pp 1454-1466
12. Forero M, Sierra-Ballen E, 'Automatic sputum colour image segmentation for tuberculosis diagnosis', *SPIE4471*, 2001
13. Forero M, Sroubek F, Cristobal G, 'Identification of tuberculosis bacteria based on shape and color', *Real-Time imaging*, 10, 2004, pp 251-262
14. Fu K.S & Mui J.K, 'A survey on image segmentation', *Pattern Recognition*, 13, 1981, pp 3-16
15. Geusebroek J, Cornelissen F, Smeulders A, Geerts H, 'Robust focusing in Microscopy', *Cytometry*, 2000, 39, pp 1-9
16. Gonzalez R and Woods R, 'Digital Image Processing', Addison-Wesley, 1992

17. Hsieh H, Marrinucci D, Bethel K, Curry D, Humphrey M, Krivacic R, Kroener J, Kroener L, Ladanyi A, Lazarus N, Kuhn P, Bruce R, Nieva J, 'High speed detection of circulating tumor cells', *Biosensors and Bioelectronics*, 2006, Article in press
18. Ihlow A, Seiffert U, 'Microscope colour image segmentation for resistance analysis of barley cells against powdery mildew', 9. Workshop "Farbbildverarbeitung", ZBS, Report No. 3/2003, Ostfildern-Nellingen, Germany, October, 2003, pp 59-66
19. International Union Against Tuberculosis and Lung Disease (IUATLD) 'Management of Tuberculosis. A guide for low income countries', Fifth edition, 2000
20. Jantzen J, 'Tutorial On Fuzzy Logic', Tech. report no 98-E 868, Technical University of Denmark, 2004
21. Jawahar C. V, Biswas P. K, Ray A. K, 'Analysis of Fuzzy Thresholding Schemes', *Pattern Recognition*, 33, 2000, pp 1339-1349
22. Kapur J. N, Sahoo P. K, Wong A. K. C, 'A new method for gray-level picture thresholding using the entropy of the histogram', *Comput. Vision Graphics Image Process.*, Vol. 29, 1985, pp 273-285
23. Kautsky J, Flusser J, Zitova B, Simberova S, 'A new wavelet-based measure of image focus', *Pattern Recognition Letters,* 23, 2002, pp 1785-1794
24. Kehtarnavaz N, Oh H.-J. 'Development and real-time application of a rule-based auto-focus algorithm', *Real-Time imaging*, 9, 2003, pp 197-203
25. Lamchiagdhase P, Preechaborisutkul K, Lomsomboon P, Srisuchart P, Tantiniti P, Khan-u-ra N, Preechaborisutkul B, 'Urine sediment examination: A comparison between the manual method and the iQ200 automated urine microscopy analyzer', *Clinica Chimica Acta*, 358, 2005, pp 167-174
26. Lumenera Corporation Data sheets for LU200 and LU130 Digital Camera Models. June 2005
27. McKeogh L, Sharpe J, Johnson K, 'A low-cost automatic translation and autofocusing system for a microscope', *Measurement, Science and Technology*, 6, 1995, pp 583-587
28. Merriam-Webster, 'Online Medical Dictionary', 2005, http://www2.meriam-webster.com
29. MATLAB Version 6.5, Release 13, Help Notes, 2002
30. Nicolls F. 'The Development of a Predictive Autofocus Algorithm using a General Image Formation Model', MSc(Eng) Thesis, University of Cape Town, 1995
31. Olabarriaga S. D, Smeulders A. W. M, 'Interaction in the segmentation of medical images: A survey', *Medical Image Analysis,* Vol. 5, 2001, pp 127-142
32. Pal S. K, King R. A, Hashim A. A, 'Automatic grey level Thresholding through index of fuzziness and entropy', *Pattern Recognition Letters*, No. 1, 1983, pp 141-146
33. Pal N. R, Pal S. K, 'A Review on Image Segmentation Techniques', *Pattern Recognition*, Vol. 26, No. 9, 1993, pp 1277-1249

34. Papik K, Molnar B, Schaefer R, Dombovari Z, Tulassay Z, Feher J, 'Application of neural networks in medicine – a review', *Med. Sci. Monit.*, 4(3), 1998, pp 538-546
35. Prismatic Project Management Team, 'Assessment of automated primary screening on PAPNET of cervical smears in the PRISMATIC trial' *The Lancet*, Vol. 353, 1999, pp 1381-1385
36. Santos A, Ortiz de Solorzano C, de la Pena J, Vaquero J, Malpica N, del Pozo F. 'Evaluation of autofocus functions in molecular cytogenetic analysis', *Journal of Microscopy,* 188, 1997, pp 264-72
37. Subbarao M, Choi T, Nikzad A. 'Focusing Techniques', *Optical Engineering*, 32, 1993, pp 2824-2836
38. Subbarao M, Tyan J.-K. 'Selecting the Optimal Focus Measure for Autofocusing and Depth-from-Focus', *IEEE Transactions on Pattern Analysis and Machine Intelligence*, 20, no. 8, 1998, pp 864-870
39. Svahn F. 'Tools and Methods to Obtain a Passive Autofocus System', Masters Thesis, Tekniska Högskolan Linköping, 1996, pp 9-34
40. Tizhoosh H. R, 'Image Thresholding using type II fuzzy sets', *Pattern Recognition*, 38, 2005, pp 2363-2372
41. Tobias O. J & Seara R, 'Image Segmentation by Histogram Thresholding Using Fuzzy Sets', *IEEE Transactions on Image Processing*, Vol. 11, No. 12, 2002, pp 1457-1465
42. Ulukanligil, M., Aslan, G., Tasci, S. 'A comparative study on the different staining methods and number of specimens for the detection of acid fast bacilli', *Memorias do Instituto Oswaldo Cruz*, 95(6), 2000, pp 855-858,
43. Veropoulos K, Campbell C, Learmonth G, Knight B, Simpson J, 'The Automated Identification of Tubercle Bacilli using Image Processing and Neural Computing Techniques', *Proceedings of the 8th International Conference on Artificial Neural Networks*, 2, 1998, pp 797-802
44. Veropoulos K, 'Machine Learning Approaches to Medical Decision Making', PhD (Phil.) Thesis, University of Bristol, 2001
45. WHO (World Health Organization), 'TB and HIV Clinical Manual', 1996
46. Wit P, Busscher H, ' Application of an artificial neural network in the enumeration of yeasts and bacteria adhering to solid substrata', *Journal of Microbiological Methods*, 32, 1998, pp 281-290
47. Zadeh L. A, 'Fuzzy Sets', *Inform. Control*, Vol. 8, 1965, pp 338-353

11 BIBLIOGRAPHY

- Bengtsson E, Wahlby C, Lindblad J, 'Robust cell image segmentation methods', *Pattern Recognition and Image Analysis*, 14(2), 2004, pp 157-167
- Chen T, Lu Y, 'Colour image segmentation and innovative approach', *Pattern Recognition*, 35, 2002, pp 395-405
- Cheng H, Chen Y, 'Fuzzy partition of two-dimensional histogram and its application to thresholding', *Pattern Recognition*, 32, 1999, pp 825-843
- Garrido A, Peh rez de la Blanca N, 'Applying deformable templates for cell image segmentation', *Pattern Recognition*, 33, 2000, pp 821-832
- Ihlow A, Seiffert U, 'Automating microscope colour image analysis using the Expectation Maximisation Algorithm', *Pattern Recognition Lecture Notes in Computer Science*, 2004, pp 536-543
- Nicolls F, de Jager G, Sewell B, 'Use of a general imaging model to achieve predictive autofocus in the scanning electron microscope', *Ultramicroscopy*, 69(1), 1997, pp 25-37
- Pantofaru C, Hebert M, 'A Comparison of Image Segmentation Algorithms', Robotics Institute, Carnegie Mellon University, Sept 2005
- Rooms F, Ronsse M, Pizurica A, Philips W, 'PSF Estimation with Applications in autofocus and Image restoration', *Proc. 3rd IEEE Benelux Signal Processing Symposium*, Leuven, Belgium, 2002, pp 1-4
- Russ J. C. 'The Image Processing Handbook', CRC Press Inc., 1992, pp 102-163
- Vollath D, 'Automatic focusing by correlative methods', *Journal of microscopy*, September, 1987, pp 279-288
- Zhang Y, Zhang Y, Wen C, 'A new focus measure method using moments ', *Image and Vision Computing*, 18, 2000, pp 959-965
- Zouagui T, Benoit-Cattin H, Odet C, 'Image segmentation functional model', *Pattern Recognition*, 37, 2004, pp 1785-1795

12 APPENDICES

12.1 ZIEHL-NEELSEN STAINING

This technique is also known as acid-fast staining. All *Myobacteria* (including TB i.e. *Myobacterium tuberculosis*) have a waxy coating built into their cell walls. Thus ordinary "Gram staining" bacteria dyeing procedures will not work as the dye cannot penetrate the bacterium. Thus as part of the acid-fast staining procedure, a detergent is applied to the bacteria which rids them of their waxy coat. The basic procedure for using Ziehl-Neelsen staining on a sputum slide is as follows:

1. A red dye called Carbol-Fuchsin is used first. This dye contains detergents, thus all the bacteria are stained red.
2. The bacteria are then washed with acid alcohol. All the bacteria that retain the red dye are then known as *acid-fast* bacteria.
3. A blue dye, Methylene blue, is then used on the slide. All the bacteria that are not acid-fast go blue, leaving the acid-fast bacteria red.

12.2 CALCULATING AVERAGE C_{SPREAD}

Slide Name	Red_avg	Green_avg	Blue_avg
Test3	0.4598	0.3059	0.2343
Test4	0.4383	0.3086	0.2530
Test5	0.4711	0.2999	0.2289
Test6	0.4620	0.3370	0.2729
Test7	0.4505	0.3176	0.2319
Test8	0.4512	0.3159	0.2329
Test9	0.4499	0.3179	0.2322
Test10	0.4623	0.3089	0.2288
Test11	0.4588	0.3194	0.2218
Test12	0.4740	0.2964	0.2296
Test13	0.4520	0.3180	0.2300
Test14	0.4503	0.3159	0.2338
Test15	0.4364	0.3195	0.2441
Test16	0.4546	0.3084	0.2370
Test17	0.4330	0.3256	0.2414
Test18	0.4429	0.3112	0.2460
Test19	0.4625	0.3125	0.2251
Test20	0.4513	0.2993	0.2494
Test21	0.4207	0.3256	0.2538
Test22	0.4238	0.3205	0.2557
Test23	0.4238	0.3205	0.2557
AVERAGE TB BACTERIA VALUES:	**0.44901**	**0.31450**	**0.23992**

Thus:

$$C_{spread}(\text{Average}) = \begin{bmatrix} 0.44901 & 0 & 0 \\ 0.31450 & 1 & 0 \\ 0.23992 & 0 & 1 \end{bmatrix}$$

12.3 FULL RESULTS OF COLOUR COMPENSATION THRESHOLDING

Table 17 The difference in segmentation results between segmenting the image using the image specific matrix or using the average matrix. Tested using test slides from the smart microscope.

Slide Name	Segmented image using the specific matrix	Segmented image using Average matrix
Test1	 Threshold = -5	 Threshold = -8
Test2	 Threshold = -7	 Threshold = -6

Test3	 Threshold = -5	 Threshold = -11
Test4	 Threshold = -5	 Threshold = -8
Test5	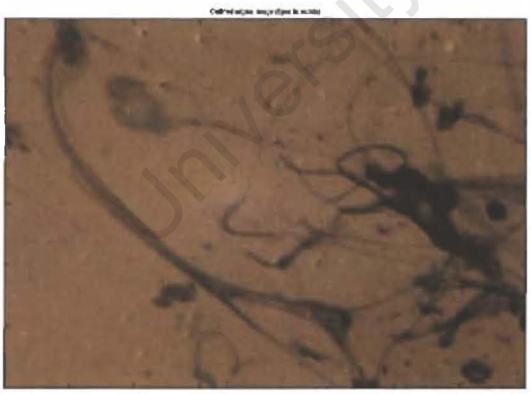 Threshold = -11	 Threshold = -11

Test6	 Threshold = -6	 Threshold = -6
Test7	 Threshold = -13	 Threshold = -12
Test8	 Threshold = -5	 Threshold = -10

Test9		
	Threshold = -5	Threshold = -6
Test10		
	Threshold = -3	Threshold = -10
Test11		
	Threshold = -13	Threshold = -13

Test12	 Threshold = -2	 Threshold = -2
Test13	 Threshold = -4	 Threshold = -2
Test14	 Threshold = -7	 Threshold = -9

Test15	 Threshold = -12	 Threshold = -8
Test16	 Threshold = -2	 Threshold = -2
Test17	 Threshold = -4	 Threshold = -5

Test18	 Threshold = -1	 Threshold = -2
Test19	 Threshold = -1	 Threshold = 2
Test20	 Threshold = -1	 Threshold = -2

12.4 CONTENTS OF THE M-FILES FOR USE IN MATLAB

12.4.1 Autofocusing

- `focusmeasures.m` – calculates the three focus measures for slides with high image content (1, 12 & 14), with medium content (2, 13 & 18) and low image content (3, 16 & 20). The output is the focus measure graphs and the time taken to run each focus measure. NOTE: This program takes a long time to run.
- `focusslide.m` – performs the focusing operations on the 20 slide series. A menu enquires which slide series the user would like to focus. The output is the grey-scale image chosen as the most in focus and the time taken to perform the focusing operation. `getim.m` is a function written for use with this program. It emulates a call to the microscope. Given the slide number and position along the z-axis, `getim.m` returns the appropriate image.

12.4.2 Segmentation

- `crispthresh.m` – performs crisp grey-scale thresholding on images. It outputs the original image with the segmented areas outlined. The image used and the threshold are changed manually in the program code.
- `fuzzyhist.m` – performs fuzzy grey-scale thresholding on images. It outputs the original image with the segmented areas outlined and a figure showing the index of fuzziness. The image used and the start and end of the initial fuzzy interval are changed manually in the program code.
- `colour_edge.m` – performs colour edge extraction on an image. `findthresh.m` is a function designed for use with this program. It finds the threshold when given the maximum value of the local maximum edge strength and all the values for the local maximum edge strength. The image used are changed at the beginning of the code.
- `colourcanny.m` – this program performs Canny edge detection on colour images. The image, σ and threshold for the Canny operator can be changed in the code. This program outputs the original image with the segmented areas outlined.
- `colourspread.m` – performs colour compensation thresholding on test images from the smart microscope. A menu enquires which test slide to segment, and then outputs the image segmented using the specific matrix for that slide and the image segmented using the average matrix.